Gas Production From a Cold, Stratigraphically Bounded Hydrate Deposit at the Mount Elbert Site, North Slope, Alaska

G.J. Moridis[1], S. Silpngarmlert[2], M.T. Reagan[1], T. Collett[3], and K. Zhang[1]
[1]*Lawrence Berkeley National Laboratory, 1 Cyclotron Rd., Berkeley, CA 94720*
[2]*ConocoPhillips, P.O. Box 2197, Houston, TX 77252*
[3]*U.S. Geological Survey, Denver Federal Center, Box 25046, MS-939, Denver, CO 80225*

Abstract
As part of an effort to identify suitable targets for a planned long-term field test, we investigate by means of numerical simulation the gas production potential from unit D, a stratigraphically bounded (Class 3) permafrost-associated hydrate occurrence penetrated in the Mount Elbert well on North Slope, Alaska. This shallow, low-pressure deposit has high porosities (ϕ = 0.4), high intrinsic permeabilities ($k = 10^{-12}$ m^2) and high hydrate saturations (S_H = 0.65). It has a low temperature (T = 2.3 – 2.6 ^{o}C) because of its proximity to the overlying permafrost. The simulation results indicate that vertical wells operating at a constant bottomhole pressure would produce at very low rates for a very long period. Horizontal wells increase gas production by almost two orders of magnitude, but production remains low. Sensitivity analysis indicates that the initial deposit temperature is by the far the most important factor determining production performance (and the most effective criterion for target selection) because it controls the sensible heat available to fuel dissociation. Thus, a 1 ^{o}C increase in temperature is sufficient to increase the production rate by a factor of almost 8. Production also increases with a decreasing hydrate saturation (because of a larger effective permeability for a given k), and is favored (to a lesser extent) by anisotropy.

Keywords
hydrates; permafrost; methane; gas production

1. Introduction

1.1. Background
Gas hydrates are solid crystalline compounds in which gas molecules (referred to as guests) occupy the lattices of ice crystal structures (called hosts). Their formation and dissociation is described by the general equation

$$G + N_H H_2O = G \bullet N_H H_2O,$$

where N_H is the hydration number, and G is a hydrate-forming gas. Natural hydrates in geological systems contain G = CH_4 as their main gas ingredient, and occur in two distinctly different geologic settings where the necessary conditions of low T and high P exist for their formation and stability: in the permafrost and in deep ocean sediments.

Although the magnitude of the CH_4 resource trapped in hydrates is the subject of rigorous debate, and the estimates vary widely between 10^{15} and 10^{18} ST m^3 (Sloan and Koh, 2008; Milkov, 2004; Klauda and Sandler, 2005), there is general consensus that it is huge, easily exceeding the total energy content of the known conventional fossil fuel

resources. Even if only a fraction of the most conservative estimate of the resource is recoverable, the CH_4 amounts involved are sufficiently large to demand evaluation of the hydrate potential as an energy source (Makogon, 1987; Dallimore et al., 1999; 2005). To that end, a global effort is currently in progress to assess the resource (Moridis et al., 2008a), and the ever-increasing global energy demand, the dwindling conventional fossil hydrocarbon reserves, and the environmental desirability of CH_4 as a fuel have added to the impetus for this effort. As result, there has been a proliferation of recent studies evaluating the technical and economic feasibility of gas production from natural hydrate accumulations, e.g., Moridis, 2003; Moridis et al., 2004; Hong and Darwish-Pooladi, 2005; Sun and Mohanty, 2005; Moridis et al., 2007a; Moridis and Sloan, 2007; Moridis and Reagan, 2007a;b;c; Moridis et al., 2008b; Kurihara et al., 2005; 2008.

Gas can be produced from hydrates by inducing dissociation via one of the three main dissociation methods (Makogon, 1997) or combinations thereof: (1) depressurization below the hydration pressure P_e (as defined by the Lw-H-V and I-H-V three-phase lines in Figure 1.1) at the temperature T, (2) thermal stimulation, based on raising T above the hydration temperature T_e at the prevailing pressure P, and (3) the use of inhibitors (such as salts and alcohols) that shift the P_e-T_e equilibrium.

1.2. Objectives and approach

This investigation is part of an effort led by the U.S. Department of Energy to identify appropriate targets for a long-term field test of production from permafrost-associated hydrate deposits (Boswell et al, 2008). The main objectives of this study are (a) to evaluate the gas production potential of the unit D hydrate accumulation at the Mount Elbert site, North Slope, Alaska, and, should this be deemed unsatisfactory, (b) to determine through sensitivity analysis the conditions and properties that can serve as criteria to identify other deposits as suitable candidate for a successful field test of production.

Unit D at the Mount Elbert site (described in more detail in Section 2) is a relatively shallow deposit that is cold (2.3 – 2.6 ^oC) because of its proximity to the permafrost. It is a typical Class 3 deposit, i.e., it involves a single zone – the hydrate-bearing layer (HBL), confined by near-impermeable top and bottom boundaries – and is characterized by the absence of an underlying zone of mobile fluids. As discussed in detail by Moridis and Reagan (2007a,b), depressurization appears to be the production method of choice because of its simplicity, its technical and economic effectiveness, the fast response of hydrates to the rapidly propagating pressure wave, the near-incompressibility of water, and the large heat capacity of water. The latter plays a significant role in providing part of the heat needed to support the strongly endothermic dissociation reaction.

Because of the high initial hydrate saturation S_H in the HBL, the effective permeability k_{eff} is very low and constant-rate production is not feasible, while pure thermal stimulation is an unattractive option because of its limited effectiveness for reasons discussed in detail by Moridis and Reagan (2007a). Thus, our studies focused exclusively on production under a constant bottomhole pressure P_w regime because earlier studies (Moridis and Reagan, 2007a; Reagan et al., 2008) had indicated this to be a promising (and possibly the only) option in production from Class 3 deposits of similar attributes. We investigated the performance of both vertical and horizontal wells, and we

conducted a sensitivity analysis to determine the most important factors affecting production.

2. The Mount Elbert Site

2.1. Regional Geological System Description

The geology and petroleum geochemistry of the rocks on the North Slope of Alaska where gas hydrates are encountered are described in considerable detail in a number of publications (Bird and Magoon, 1987; Collett, 1993). The first direct confirmation of gas hydrate on the North Slope was provided by data from a single well (the Northwest Eileen State-2 well, located in the northwest part of the Prudhoe Bay Field), in which studies of pressurized core samples, downhole logs, and production testing had confirmed the occurrence of three gas-hydrate-bearing stratigraphic units (Collett, 1993). Analysis of downhole log data from an additional 50 exploratory and production wells in the same area provided additional indications of hydrate occurrence in six laterally continuous sandstone and conglomerate units (A to F), which are all confined to the geographical area shown in Figure 2.1. Collett (2007) indicated that the hydrate units appear to trap down-dip several large free-gas accumulations (Figure 2.1; units A through D). The volume of gas within the Eileen Gas Hydrate Accumulation (Collett, 2007) is estimated at about twice the volume of known conventional gas in the Prudhoe Bay Field (Collett, 1993), and ranges between 1.0×10^{12} and 1.2×10^{12} m^3 STP (Collett, 2007).

2.2. Previous Studies

Previous and current studies of gas production from hydrates in the North Slope of Alaska involve collaborations that are spearheaded by BP Exploration (Alaska - BPXA), Inc., the U.S. Department of Energy, and the U.S. Geological Survey, and involve several other organizations. This effort is supported by the Methane Hydrate Research and Development Act (enacted by the U.S. Congress in 2000 and renewed in 2005), and aims to determine the viability of the North Slope hydrates as an energy source (Mount Elbert Science Team, 2007) through investigations that will culminate with a long-term (1.5-2 years) field test of gas production (Boswell et al, 2008).

Analysis of geophysical surveys and well log data led the team to the installation of a well in 2007 at a previously undrilled, fault-bounded accumulation named the "Mount Elbert" prospect to acquire critical reservoir data needed to develop a longer-term production test program. The Mount Elbert-01 well was drilled to a depth of 915 m using chilled oil-based drilling fluid to avoid the inhibitor-induced dissociation caused by the salts and alcohols in conventional muds. A remarkable achievement was the recovery of significant lengths of core from the hydrate intervals, which were used for subsequent analyses of pore water geochemistry, microbiology, gas chemistry, petrophysical properties, and thermal and physical properties. After a battery of well log surveys was completed, a Schlumberger Modular Dynamic Testing (MDT) was conducted in two reservoir-quality sandy hydrate-bearing sections with high S_H (60% to 75%). Gas was produced from the gas hydrates in each of the tests. This study has yielded one of the most comprehensive datasets yet compiled on a naturally occurring gas hydrate geologic deposit (Collett, 2007).

Extensive discussions of the Mount Elbert geology and analyses of the various tests conducted at the site are presented in various papers in this volume (Boswell et al., 2009).

2.3. The unit D Hydrate Deposit

Figure 2.2 shows units C and D at the Mount Elbert site, and Figure 2.1 shows their location relative to (a) the permafrost and (b) the predicted base of the methane hydrate stability zone. Unit D is a shallow permafrost-associated hydrate deposit, with a HBL beginning at a depth of z = -616.6 m. The deposit is about 11.3 m thick, is bounded by nearly impermeable shale layers, and has high porosity, permeability and hydrate saturation (Winter et al, this volume). Because of its proximity to the permafrost, its temperature is low, ranging between T_T = 2.3 ^{o}C and T_B = 2.6 ^{o}C at the HBL top and bottom, respectively. The pressure at the HBL top is a low P_T = 6.386 MPa. The properties and initial conditions of the unit D and its boundaries are listed in Table 1.

In terms of desirability as a production target for a long-term production test, our initial perception of the advantage of unit D over unit C was that it is a Class 3 deposit, i.e., it is characterized by the absence of an underlying zone of mobile fluids, as opposed to unit C, which is connected to a deep, extensive aquifer that makes depressurization challenging and water disposal an additional complication. Continuing studies have provided indications that unit D is likely in communication with some underlying water-bearing sand sections, but the extent of this communication is unknown. For the purpose of this study, the production modeling is based on the assumption that unit D is a Class 3 deposit with no connection to a underlying zone of mobile fluids.

Compared to unit D, unit C is thicker and warmer by about 1 ^{o}C (Collett et al., this volume, b). Although this may initially appear unimportant, the small increase in temperature can make a very significant difference in production from hydrates because it increases the sensible heat that is available to support the endothermic hydrate dissociation: the lower the initial temperature T, the bigger the potential effect of an additional 1 ^{o}C on dissociation and gas production.

Units C and D have similar properties, and similar S_H. Because of the MDT test that was conducted within the C unit, it was possible to determine some of its in-situ properties by history matching the MDT data (Anderson et al., 2008; Anderson, this volume). Other unit C and unit D properties and conditions were determined from well log analyses and core studies of samples retrieved during drilling (Collett et al., this volume b).

3. The Numerical Models and Simulation Approach

3.1. The numerical simulation code

We used the TOUGH+HYDRATE simulator (Moridis et al., 2008c; Zhang et al., 2008) to conduct the numerical studies in this paper. This code (hereafter referred to as T+H) can model all the known processes involved in the system response of natural CH_4-hydrates in complex geologic media, including the flow of fluids and heat, the thermophysical properties of reservoir fluids, thermodynamic changes and phase behavior, and the non-isothermal chemical reaction of CH_4-hydrate formation and/or dissociation, which can be described by either an equilibrium or a kinetic model (Kim et al., 1998; Clarke and Bishnoi, 2001; Moridis and Kowalsky, 2008). T+H is a compositional simulator, and its formulation accounts for heat and up to four mass components (i.e., H_2O, CH_4, CH_4-hydrate, and water-soluble inhibitors such as salts or

alcohols) that are partitioned among four possible phases: gas, aqueous liquid, ice, and hydrate. The T+H code can describe all the 15 possible thermodynamic states (phase combinations) of the CH_4+H_2O system and any combination of the three hydrate dissociation methods. It can handle the phase changes, state transitions, strong nonlinearities and steep solution surfaces that are typical of hydrate dissociation problems. Because of the very large computational requirements of this type of problem and the use of very large grids (see Section 3.3), we used the distributed-memory, massively parallel version of the code (Zhang et al., 2008) in the simulations discussed in this paper.

3.2. System geometry. The geologic system in this study corresponds to a location at the Mount Elbert site where the top of the HBL is at a depth of z = -616.6 m. This is a typical Class 3 deposit, in which the 11.3-m-thick HBL is overlain and underlain by nearly impermeable boundaries, i.e., shale strata. Based on experienced gained in earlier studies (Moridis and Reagan, 2007a;b; Moridis et al., 2008b) and preliminary scoping calculations, the simulation domain was extended 30 m into the overburden and underburden of the HBL, a distance that was deemed sufficient to allow accurate heat exchange with the deposit during the production period.

We investigated the performance of both a single vertical and a single horizontal well producing from sections (cylindrical and rectangular) of the same hydrate deposit, using the same surface area and including the same hydrate volume in each simulation configuration. The outer radius of the cylindrical section was r_{max} = 400 m, corresponding to a well spacing of 50 ha (125 acres). The rectangular section with the same area and hydrate volume had a square footprint with a side L_y = 709 m. The geometry and well configuration of these two Class 3 systems are shown in Figures 3.1 and 3.2. The horizontal well was placed at the top of the HBL to capitalize on gas buoyancy and accumulation at this location, in addition to minimizing water production (Z_W = 0, see Figure 3.2). Both the vertical and the horizontal well had a radius r_w = 0.1 m.

3.3. Domain discretization. For maximum accuracy, very fine grids were used in the simulation of production from both the cylindrical and rectangular sections of the hydrate deposit. The cylindrical domain of Figure 3.1 was discretized into 200 x 300 = 60,000 gridblocks in (r,z), resulting in a system of 240,000 equations. Discretization along the radial direction was non-uniform, increasing logarithmically from r_w to r_{max}, with Δr_0 = 0.05 m. Discretization along the z-axis was uniform (with Δz = 0.1 m) within the HBL and its immediate vicinity, but non-uniform (with Δz increasing) near the top and bottom of the domain.

In the study of the performance of the horizontal well, we used only a single slice of unit thickness on the (x,z) plane, i.e., perpendicular to the horizontal well (Figure Y). Implicit in this approach is the assumption of uniformity along the well length L_w, i.e., along the y-axis. While this assumption may not be always valid in light of expected pressure variations along the length of the well, it is a good first-order approximation, it can be used to bound the expected solution through the choice of an appropriate range of well pressures in the studied slices, and it allows high-definition in the description of the system behavior without resulting in a prohibitively large grid. As in the case of production from a single vertical well in a cylindrical section of the hydrate deposit, the

2D domain in (x,z) was discretized into 200 x 300 = 60,000 gridblocks in (x,z). The vertical discretization was the same as in the case of the cylindrical system. Discretization along x-axis was non-uniform, increasing logarithmically from $x_0 = r_w$ to L_x, with Δx_0 = 0.05 m.

Such a fine discretization is important (and possibly necessary) for accurate predictions when solid phases such as ice and hydrates are involved (Moridis et al., 2007). This high degree of refinement provided the level of detail needed to capture important processes near the wellbore and in the entire hydrate-bearing zone. Assuming an equilibrium reaction of hydrate dissociation during this long-term production process (Kowalsky and Moridis, 2007), and accounting for the water salinity, the grid resulted in 240,000 coupled equations that were solved simultaneously.

3.4. System properties and well description. The hydraulic and thermal properties of the various geological media (the HBL and the confining layers) in unit D, as well as the initial conditions, were obtained from data based on the first field test at the site (Anderson et al., 2008), and are listed in Table 1. We assumed that the initial hydrate and aqueous saturations (S_H and S_A, respectively) were uniformly distributed in the HBL, and that the overburden and underburden had both the same properties. The relative permeability relationships and the corresponding parameters were based on data obtained from history matching of the results of MDT test that had been conducted at the C unit at the same site (Anderson et al., 2008), which appeared to have similar properties. The capillary pressure relationships and parameters were determined from the particle size analysis of porous media samples from the deeper (but similar) C unit (White, 2008) and were consistent with the porosity, ϕ, and permeability, k, of the D unit.

The importance of the near-well region dictated the physical representation of the wellbore in the vertical well study. To avoid a theoretically correct but computationally intensive solution of the Navier-Stokes equation, we approximated wellbore flow by Darcian flow through a pseudo-porous medium describing the interior of the well. Earlier studies had shown the validity of this approximation (Moridis and Reagan, 2007b;c). This pseudo-medium had $\phi = 1$, a very high $k = 10^{-9}$-10^{-8} m^2 (=1,000-10,000 Darcies), a capillary pressure $P_c = 0$, a relative permeability that was a linear function of the phase saturations in the wellbore, and a low (but nonzero) irreducible gas saturation $S_{irG} = 0.005$ (necessary to allow the emergence of a free gas phase in the well).

3.5. Initial and boundary conditions. The no-flow conditions (of fluids and heat) that were applied at the reservoir outer boundaries (at a radius $r = r_{max}$ and at $x = L_x = L_y$ /2, See Figures 3.1 and 3.2) implied the presence of other wells with the same characteristics in adjacent sections of the hydrate deposit on the same spacing patterns.

We determined the initial conditions in the reservoir by following the initialization process described by Moridis and Reagan (2007a;b). The temperatures at the top and bottom of the HBL (T_T and T_B, respectively) have been extrapolated from high resolution equilibrated temperature log surveys in a nearby well (Collett et al., this volume b). In both the cylindrical and the rectangular systems, the uppermost and lowermost gridblock layers (i.e., at the top of the overburden and at the bottom of the underburden in the simulated domains, where Δz = 0.001 m) were treated as boundaries with constant conditions and properties. The temperatures at the upper and lower domain

boundaries (T_U and T_L, respectively) were determined through a trial-and-error simulation process that resulted in the known T_P and T_B across the HBL. Note that the shales in the overburden and underburden were treated as impermeable (Table 1).

Knowing (a) the depth at the base of the HBL, and (b) assuming that the pressures in the subsurface follow the hydrostatic distribution—a hypothesis supported by field observations (Collett et al., 1988) and other observations (Wright et al., 1999) in hydrate accumulations—we determined the pressure P_T (at z = -616.6 m, see Figures 3.1 and 3.2) using the P-, T- and salinity-adjusted water density (1005 kg/m^3 at atmospheric pressure). Then, using P_T and the boundary temperatures T_T and T_B, the hydrostatic gradient and representative thermal conductivity values were employed to determine the P- and T-profiles in the domains by means of a short simulation.

For reasons explained in detail by Moridis and Reagan (2007b), depressurization appears to be the most effective dissociation strategy, and a constant-pressure regime (involving a constant bottomhole pressure P_w at the well) is the most promising method of gas production from Class 3 hydrate deposits. Its numerical representation involves treating the well as an internal boundary. In the case of a vertical well, this boundary is placed in the gridblock above the uppermost cell in the well. By imposing a constant P_w, a thermal conductivity k_Θ = 0 W/m/K, and a realistic (though unimportant) constant temperature T_w at this internal boundary, the correct constant-P condition was applied to the well while avoiding any non-physical temperature distributions in the well itself (the large advective flows into the uppermost gridblock from its immediate neighbor eliminated any unrealistic heat transfer effects that could have resulted from an incorrect k_Θ and/or T_w). In our study, the P_w = 3.0 MPa exceeds the pressure at the quadruple point P_Q, thus eliminating the possibility of ice formation and the corresponding potentially adverse effect on k_{eff}.

3.6. Simulation process and outputs. The maximum simulation period was initially the typical 30-year life span of a well, but it had to be extended to 50 years in the case of the horizontal well in order to investigate its very-long-term performance. In the course of the simulation, the following conditions and parameters were monitored: Spatial distributions of P, T, and gas and hydrate phase saturations (S_G and S_H); Volumetric rate of CH_4 released from dissociation and of CH_4 production at the well (Q_R and Q_P, respectively); Cumulative volume of CH_4 released from dissociation, produced at the well, or remaining in the deposit as free gas (V_R, V_P and V_F, respectively); water mass production rate at the well (Q_W) and cumulative mass of produced water (M_W); the remaining hydrate as a fraction of its original mass ($M_{HR} = M_{H,t}/ M_{H,0}$, where $M_{H,0}$ and $M_{H,t}$ are the hydrate mass in the reservoir at times 0 and t, respectively).

4. The Case of Production Using a Vertical Well

4.1. Gas production

Figure 4.1 shows the evolution of Q_R and Q_P from the single vertical well at the center of the cylindrical reservoir of Figure 3.1 over time. The most important conclusion from the review of Figure 4.1 is that the CH_4 release and production remain very low for a very long period. Thus, Q_R and Q_P < 7x10^{-4} ST m^3/s (< 2000 ST ft^3/s) for 8,000 days, i.e., almost 22 years. After that time, both Q_R and Q_P appear to increase exponentially with

time, but are lower than 2.3×10^{-3} ST m^3/s (= 7000 ST ft^3/s) even after t = 10,800 days (30 years). The low production rate is caused by the very low initial temperature of the hydrate in the HBL. The low T reduces the rate of the dissociation reaction and severely reduces the sensible heat that is available to support it. The cumulative produced volume V_P in Figure 4.2 provides further confirmation of the limited potential of unit D as a target for production from hydrates by depressurization: after continuous production for t = 30 years, a mere $V_P = 5.3 \times 10^5$ ST m^3 (=1.9×10^7 ST ft^3) of CH_4 have been produced.

An interesting observation from Figures 4.1 and 4.2 is that gas release from dissociation lags production for a very long time. Thus, $Q_P > Q_R$ for t < 9,000 days (Figure 4.1), and $V_P > V_R$ even at the end of the 30-year-long production period (Figure 4.2). The source of the additional gas is dissolved CH_4 that is released from solution as the pressure in the formation drops (and the CH_4 solubility decreases) during production. Note the very low level of free gas, V_F, in the reservoir during production (Figure 4.2), which does not exhibit an upward trend until the time of the rapid increase in Q_R and Q_P (Figure 4.1). The low levels of V_F, and the near-parity of V_R and V_P (and Q_R and Q_P), indicate that there is little gas accumulation in the reservoir, and most of the gas released from dissociation and dissolution is produced at the vertical well. After t = 9,000 days, we see that gas release begins to outpace gas production, indicating that hydrate dissociation has finally begun to create significant free gas in the reservoir (as depressurization has finally destabilized the cold, stable initial state of the system), allowing production to increase exponentially.

4.2. Water production and effectiveness of dissociation

The water production rate Q_W in Figure 4.3 remains at low levels and within a very narrow range (0.02 kg/s < Q_W < 0.026 kg/s) during the entire 30-year production period. The relative stability of Q_W leads to the near-linear appearance of the cumulative water mass M_W curve. It is obvious that M_W is at easily manageable levels.

Of particular interest is the evolution of M_{HR} in Figure 4.4, which indicates that barely 0.2% of the total hydrate mass in the HBL has dissociated at the end of the production period. In practical terms, this indicates that 30 years of continuous production have not even made a dent to the original hydrate mass. This is unequivocally demonstrated by the spatial distributions of the phase saturations shown in Figure 4.5. The staircase appearance of the M_{HR} is the result of the very limited dissociation, to the point that discretization effects become evident: dissociation and hydrate depletion are characterized by very sharp fronts and occur in very few gridblocks, with their numbers too limited to result in a smoother curve.

4.3. Phase saturations and overall evaluation

The S_H distribution at t = 30 years (Figure 4.5) depicts hydrate destruction that is minimal in extent and concentrated in the vicinity of the well at the top and bottom of the HBL, consistent with the very late onset of significant gas release in the reservoir seen in Figure 4.1. The spatial distribution of S_G in Figure 4.5 is consistent with the low V_F levels of Figure 4.2. It is defined by (a) the accumulation of high-S_G gas in a limited zone at the top of the HBL, (b) very low S_G below the gas bank for r < 50 m, and (c) S_G = 0 in the rest of the profile. Drainage of water originating from dissociation and buoyancy of the

released gas are the reasons for the absence of a zone of significant S_G at the bottom of the HBL near the well, even though the S_H profile shows evidence of dissociation.

Clearly, gas production from such a relatively cold, permafrost-associated, Class 3 deposit using vertical wells appears to be very ineffective, with little (if any) hope of attaining commercial viability. In the ensuing sections, we investigate the use of horizontal wells (operating at a constant P_w) as an alternative production strategy.

5. The Case of Production Using a Horizontal Well

5.1. Gas production

Figure 5.1 shows the evolution of Q_R and Q_P from a horizontal well (described in Figure 3.2) over time, and includes for reference the Q_R and Q_P corresponding to the vertical well (from Figure 4.1). The use of the horizontal well is shown to increase both Q_R and Q_P by about two orders of magnitude. While the improvement in performance over the vertical well is dramatic, Q_P remains low in absolute terms. However, it is possible that the production outlook may improve with longer wells, different well configurations, more complex production strategies, and by the consideration of heterogeneity (which has been shown to improve production in layered systems such as the ones in units C and D of Mount Elbert – see Kurihara et al., 2005; 2009).

The evolution of Q_R and Q_P is characterized by an initial short period (Stage 1, to t = 670 days) of rapid increase, is succeeded by a long period of continuous but mild increase (stage 2) that lasts until t = 16,300 days (i.e., almost 45 years), and is followed by a period of continuous mild decline (Stage 3). At the end of Stage 1, $Q_P = 1.34\text{x}10^{-2}$ ST m^3/s (= $4.1\text{x}10^4$ ST ft^3/day), and peaks at the end of Stage 2, when $Q_P = 5.35\text{x}10^{-2}$ ST m^3/s (= $1.63\text{x}10^5$ ST ft^3/day).

Stage 1 is associated with rapid depressurization (especially near the wellbore) and corresponds to the rapid advancement of the depressurization front in the deposit (as will be shown in Section 5.3). Because (a) the pressure drop $\Delta P = P_0 - P_w$ between the bottomhole pressure and the pressure at the dissociation front is at its maximum ΔP_{max} in the HBL, and (b) dissociation expands continuously into unaffected parts of the HBL as the depressurization front advances quickly, Q_R and Q_P increase rapidly and dQ_R/dt and dQ_P/dt are at their maximum. The endothermic nature of the hydrate dissociation reaction results in cooling of the HBL, but this has a limited effect in countering the effects of maximum ΔP on subsequent dissociation.

The end of Stage 1 and onset of Stage 2 is marked by the depressurization front reaching the outer boundaries of the HBL domain (i.e., at $y = L_y$, $x = L_x$). When this happens, the pressure wave can no longer advance, and the pressure drop at any point in the domain $\Delta P = P - P_w < \Delta P_{max}$. While Q_R and Q_P continue to increase because a larger volume of hydrate is dissociating, they do so slower, i.e., the lower pressure gradient leads to the reduction in dQ_R/dt and dQ_P/dt, which remain positive. Additionally, continuing HBL cooling caused by advancing hydrate dissociation makes further dissociation progressively more difficult.

Finally, the continuously diminishing driving force of dissociation (i.e., the ΔP) and the parallel reduction in the sensible heat that fuels and supports it lead to the declining Q_R and Q_P in Stage 3, which is characterized by negative dQ_R/dt and dQ_P/dt (Figure 5.1). Because of the low T of the HBL in our study and, consequently, Q_R and Q_P are low in relation to the total hydrate mass, there is significant delay in the onset of

Stage 3, and production increases monotonically and continuously over almost 45 years of production.

Q_R and Q_P in Figure 5.1 are very similar in magnitude, as was the case in production from a vertical well. Unlike the vertical well case, $Q_R > Q_P$ in production from the horizontal well. We observe a similar pattern in the relationship of V_R and V_P in Figure 5.2, with V_R being very slightly larger than V_P, while both (and V_F) are about two orders of magnitude larger than the ones corresponding to the vertical well case. Review of the relative magnitudes of Q_R, Q_P, V_R, V_P, and V_F confirms the pattern identified in the vertical well case, i.e., little gas accumulation in the reservoir, with most of the gas released from dissociation and dissolution is produced at the horizontal well. The cumulative produced volume V_P in Figure 5.2 provides further confirmation of the improved outlook, but also of the challenge of unit D as a target for production from hydrates by depressurization: after continuous production for t = 50 years, $V_P = 5.3 \times 10^7$ ST m^3 ($=1.9 \times 10^9$ ST ft^3) of CH_4 have been produced. While this is a tremendous improvement over the vertical well case, it is still low in absolute terms.

5.2. Water production and effectiveness of dissociation

The water production rate Q_W in Figure 5.3 shows some fluctuations at very early times (T < 100 days), but it then stabilizes at a low level and decreases slowly over the 50-year production period. During the entire time, Q_W is confined within a very narrow range (0.8 kg/s < Q_W < 1.3 kg/s), and its declining long-term trend is (a) an inevitable consequence of a continuously declining pressure differential ΔP, and (b) consistent with observations and conclusions from previous studies of production from hydrates (Moridis et al, 2007a;b). Of interest is the near parallel appearance of the cumulative water mass M_W curves in the horizontal and vertical cases. While M_W is larger (as expected) in the horizontal well case, it remains at manageable levels.

Review of the evolution of M_{HR} in Figure 5.4 provides additional evidence of the significant improvement in the effectiveness of dissociation using a horizontal well. Thus, about 9% of $M_{H,0}$ has been destroyed at t = 30 years, and the number rises to slightly over 20% after t = 50 years. While these numbers are respectable, they remain low when compared to production from conventional gas reservoirs employing horizontal wells of similar size. The inevitable conclusion is that, while horizontal wells are orders of magnitude more effective than vertical ones in gas production from hydrate deposits, relatively cold, permafrost-associated hydrates are challenging targets. Barring new developments in the technology of production from hydrates and changes in the pricing environment of natural gas, it is possible that such deposits may only hold promise as very-long-term, low- Q_P reservoirs.

5.3. Spatial distributions

The evolution of the spatial distribution of S_H in Figure 5.5 shows a dissociation pattern that is clearly far more extensive than that of the vertical well, but which is still limited compared to other studies involving much warmer deposits (Moridis and Reagan, 2007b). The minor dissociation observed until t = 720 days reflects the low T_0 of the unit D deposit. Note that significant hydrate dissociation occurs at the two main locations identified in the case of the vertical well: mainly at the HBL top, where the horizontal well is located (and where depressurization is at its maximum), and to a much lesser

extent along the base of the HBL because of continuing geothermal heat inflows from the underburden.

The S_G distribution over time in Figure 5.6 is consistent with the relatively low dissociation and limited gas accumulation indicated by Figures 5.1 and 5.2, and depicted by Figure 5.5. It takes a very long time (t = 720 days) for gas to accumulate at discernible saturation levels in the HBL. When this happens, it is limited to a thin gas zone at the top of the HBL. Unlike the case of the vertical well (in which the penetration of the entire HBL made possible the emergence of a free-gas zone at very low (almost trace) S_H levels at the base of the HBL, see Figure 4.5), the significant physical separation of the horizontal well from the bottom of the HBL prevents the emergence of even traces of gas at this location because of buoyancy of the gas released from dissociation (rising to the top), and drainage of the water released along the entire HBL profile. A comparison of the S_H and S_G profiles in Figures 5.5 and 5.6 indicates that the zone of significant hydrate destruction is much smaller than the free gas zone because the water released from dissociation (rather than CH_4) occupies the newly hydrate-free space.

The T distribution in Figure 5.7 clearly describes the advancing dissociation interface as a sharp front that defines an abrupt temperature change within a narrow zone: while the T is practically undisturbed at near-T_0 levels ahead of the front until well into the production process (i.e., for t > 7,200 days), the endothermic dissociation reaction leads to a significant temperature drop behind it, i.e., in the region where depressurization is causing dissociation. The sharpness of the interface is caused by the low effective permeability k_{eff} (caused by the high initial S_H) of the HBL. As expected, the sharp front (depicted by the abrupt temperature change in Figure 5.7) moves away from the x = 0 axis in a manner that seems to correlate very well with the edges (top and bottom) of the dissociation zone depicted by the hydrate destruction in the S_H profile of Figure 5.5. The sharp T front disappears sometime after t = 7,200, when the dissociation front reaches the $x = L_x$ boundary and the entire domain begins to dissociate, albeit at a slow rate. The evolution of T over time in Figure 5.7 is consistent with expectations, with the HBL becoming progressively colder as dissociation continues.

The P distributions in Figure 5.8 show that the entire HBL experiences a significant pressure drop even at early times, which, unlike the sharp fronts that mark the T distribution, occurs in a diffuse manner over extended regions. This is caused by the high-speed of propagation of the pressure wave in porous media, which is typical of advective processes of fluid flow. Comparison of the P distribution in Figure 5.8 to the S_H and T distributions (in Figures 5.5 and 5.7, respectively) shows that the pressure front advances well ahead of the dissociation front. This is caused by the initial thermodynamic state of the hydrate in the HBL, which is quite stable, i.e., safely within the Lw+H zone and away from the base of the stability zone defined by the Lw+H+V equilibrium curve of three-phase coexistence in Figure 1.1. Because of the enhanced initial stability, a significant pressure drop has to be attained before dissociation can begin in earnest (and be marked by sharp T-fronts and disturbed S_H profiles), hence the lag in the initiation of dissociation.

6. Sensitivity Analysis

Using the HBL and horizontal well described in Section 3 and analyzed in Section 5, we investigated the sensitivity of gas production to the following conditions and parameters:

(a) The stability of the hydrate deposit, as quantified by its initial temperature T and its deviation from the equilibrium temperature at the prevailing pressure,
(b) The initial hydrate saturation S_H,
(c) The formation anisotropy, i.e., the k_V/k_H ratio of the HBL sediment.

Because the first part of this study has clearly demonstrated the limited effectiveness of vertical wells, all sensitivity-related studies involved horizontal wells of the type shown in Figure 3.2.

6.1. Sensitivity to T

Figure 6.1 shows the dramatic effect that T (as a measure of the hydrate stability at a given P) has on production. For this study, the temperature of the HBL boundaries (T_T and T_B, see Section 3.5) of the D unit was raised by ΔT = 1 ^{o}C, resulting in a similar ΔT along the entire HBL profile. The increase in Q_R and Q_P corresponding to this slight temperature rise is nothing less than spectacular, reaching a factor of almost 8 at its peak. Because of the strong enhancing effect of the higher T on dissociation, Stage 1 and Stage 2 (associated with the Q_R and Q_P peak, see Section 5.1) occur much earlier than in the reference case, and, consequently, Stage 3 (which involves slow dissociation from the entire hydrate body in the HBL in response to a mild and declining ΔP) is longer and marked by a very gradual decline in Q_R and Q_P. Figure 6.1 shows that the increase in Q_R and Q_P is most prevalent during the earlier part of the production period, i.e., during Stages 1 and 2.

The strong effect of even a slightly higher T on production is also demonstrated by Figure 6.1, which shows that V_R and V_P increase (over the reference case) by a factor which is 2.8 at its minimum (at the end of the production period), and higher earlier in the production period. In essence, these results indicate the superiority of warmer hydrate deposits as potential production targets (in terms of production and early return), and are consistent with previous observations (Moridis and Reagan, 2007a;b; Reagan et al., 2008). The increase in V_F is also significant in relative terms, but the total volume of free gas remains low (in absolute terms) and indicates that, as in the reference case, gas accumulation in the reservoir is limited because most of the released CH_4 is produced at the well.

The appeal of even slightly warmer deposits is further demonstrated by Figure 6.3, which shows that water production remains practically the same despite drastically larger Q_R and Q_P. The M_{HR} in Figure 6.4 shows that the ΔT = 1 ^{o}C difference is sufficient to reduce the remaining hydrate from 80% to 40% of $M_{H,0}$, pointing to an increase in the mass of destroyed hydrate by a factor of 3 at the end of production. This is consistent with the results of Figure 6.2, and encapsulates in a cumulative sense the appeal of warmer deposits. Further support of the superiority of warmer hydrates, in addition to visual confirmation of the results in Figures 5.2 and 5.4, is provided by the comparisons of the S_H and S_G profiles in Figures 6.5 and 6.6, which show significant more hydrate destruction and larger free gas accumulations for the case of the warmer HBL.

6.2. Sensitivity to S_H

Figure 6.7 shows that Q_P increases with a decreasing S_H, at least within the range we investigated ($0.35 \leq S_H \leq 0.65$). This is attributed to the higher k_{eff} that corresponds to lower S_H levels for a given intrinsic permeability k. Additionally, a decreasing S_H leads to correspondingly (and proportionally) shorter production Stages 1 and 2. Thus, the lowest $S_H = 0.35$ (a) has the highest Q_P that (b) occurs at the earliest time, and (c) has the longest Stage 3 (characterized by the mildest decline). The corresponding V_P vs. t curves in Figure 6.8 show that the early high Q_P rates at low S_H are sufficient to preserve higher V_P despite later reversals in the relative Q_P magnitude, and provide further confirmation of the appeal of such "lean" hydrate systems under the conditions of the unit D Class 3 deposit at the Mount Elbert site.

The water production rates Q_w in Figure 6.9 increase with a decreasing S_H. They differ by orders of magnitude for the various S_H in the study because they reflect drastically different k_{eff} regimes (strongly influenced by S_H). Q_w decreases over time because the driving force ΔP in the reservoir decreases as depressurization advances, and eventually the three Q_w appear to converge after t = 10,000 days of production. Similarly, the cumulative mass of produced water M_w increases with a decreasing S_H, but eventually the three M_w curves converge at about t = 5,000 days. The M_{HR} curve in Figure 6.10 provides a measure of the relative advantage that lower S_H confer to gas production from hydrates with the attributes if unit D, and is complementary to the results in Figure 6.8.

6.3. Sensitivity to anisotropy

Review of the evolution of the S_H distribution pattern in Figure 5.5 showed the propensity of dissociation to advance horizontally and preferentially along the top (mainly) and the bottom of the HBL because of the heat inflows from the boundaries. At the top of the HBL, this tendency was significantly enhanced by the proximity to the well, where depressurization is at its most intense, and by the favorable relative permeability to gas flow (a result of gas accumulation at this location). Given these earlier indications, the results of the effect of anisotropy (described by the ratio $k_R = k_V/k_H$) in Figure 6.11 are entirely anticipated. Decreasing k_R to 0.1 (from its original value of 1 in the reference case) creates a flow regime that enhances horizontal flow and facilitates dissociation.

Thus, Q_P during Stage 2 (the longest of the 3 production stages) is higher than that in the reference case because dissociation and horizontal flow are favored. However, because the initial flow regime around the well immediately after the initiation of production is cylindrical, Q_P at a very early stage is lower than that in the reference case, and the lower cumulative permeability delays the time of arrival of the depressurization front at the $x = L_x$ boundary and prolongs Stage 1. However, the transition into the favorable horizontal dissociation and flow regime results in a Q_P that is higher than that for $k_R = 1$ in the later part of Stage 1. The more effective dissociation for $k_R = 0.1$ leads to faster cooling, resulting in an earlier onset of Stage 3 and a lower Q_P than in the reference case.

The effect of k_R on production is depicted by the comparison of the corresponding V_F curves in Figure 6.12. At early times (t < 1,400 days), V_F for the $k_R = 1$ case exceeds that for $k_R = 0.1$. Beyond that time, the pattern reverses, and the lower k_R appears to have an advantage in long-term production. However, the increase in long-term production caused by the lower k_R is incremental and not that significant. This is further confirmed

by the evolution of M_{HR} in Figure 6.13, which shows only minor incremental hydrate destruction for $k_R = 0.1$.

The water production rates Q_w for the two k_R levels in Figure 6.14 follow the same pattern of long-term decline (a direct consequence of the declining ΔP differential), and their comparisons indicates that, all else being equal, Q_w decreases with a decreasing k_R. This is caused by the reduced permeability, which prevents the aqueous phase (widely distributed in the entire HBL, unlike the gas phase that is concentrated at the top – see Figure 5.6) from flowing easily to the well. The M_w patterns in Figure 6.14 reflect the Q_w relationship.

7. Summary and Conclusions

This study is part of an effort led by the U.S. Department of Energy to identify appropriate targets for a long-term field test of production from permafrost-associated hydrate deposits. We focus on the evaluation of the gas production potential of the unit D hydrate accumulation at the Mount Elbert site, North Slope, Alaska, a shallower and colder Class 3 deposit than the unit C deposit. We investigate the performance of vertical and horizontal wells operating under constant bottomhole pressure in gas production fueled by depressurization-induced dissociation of the hydrates. Based on the results of this study, we draw the following conclusions:

(1) The effectiveness of vertical wells operating at a constant P_w in the low-P, low-T unit D deposit is very limited. Gas production from this hydrate accumulation is hampered by very low rates that persist for very long times

(2) Horizontal wells operating at a constant P_w appear to yield higher production rates relative to vertical wells in the cold hydrate deposit of unit D at the Mount Elbert site. Although production using horizontal wells is about two orders of magnitude larger than that from vertical wells accessing the same section of the HBL, it is still low in absolute terms, and carries the additional burden of the significantly higher costs of installing and operating a horizontal well.

(3) Water production in either the vertical or the horizontal well case remains well within manageable limits.

(4) It is possible that the production rates may improve with the use of longer wells, the use of different well configurations, and the development of more complex strategies to deliver more efficient dissociation. Such new developments and solutions are not evident. Although the authors are aware of some new ideas that have been proposed to address these issues, their technical feasibility has not been explored (let alone established), and their potential effectiveness in increasing gas production has yet to be evaluated.

(5) The sensitivity analysis we conducted identified the desirable features, to be used as criteria for the selection of a hydrate deposit as an appropriate production target. The sensitivity of gas production to the initial HBL temperature is nothing short of dramatic: a $\Delta T = 1\ ^{o}$C increase results in a 8-fold increase in Q_P, and in a 3-fold (at least) increase in the V_P, while water production is practically unaffected. Confirming earlier studies (Moridis and Reagan, 2007a;b; Moridis et al., 2008b), temperature emerges again as the most important factor affecting gas production, and its importance appears enhanced in the case of colder deposits.

These results and observations guide us to select the deepest, warmest hydrate deposit (i.e., with the highest sensible heat and affording the largest possible pressure gradient ΔP) as the most promising production target from among those accumulations that meet other basic criteria of reservoir quality and accessibility.

(6) All other things being equal, hydrate accumulations with low S_H appear to be more desirable potential targets for a successful long-term field test of production from colder, permafrost-associated hydrates because of their tendency to yield higher Q_P at early times that are well within the time frame of the planned test. Water production increases with a decreasing S_H, but converges to the same level in the long run.

(7) Anisotropy is not a feature that is readily observable, and is difficult to use as a criterion for the selection of an appropriate hydrate deposits as a production target. If there is evidence of anisotropy caused by external factors (such as sedimentation patterns, which usually result in $k_R < 1$), this is expected to lead to higher gas production (and lower water production) within the time frame of the planned field test.

Acknowledgment

This work was supported by the Assistant Secretary for Fossil Energy, Office of Natural Gas and Petroleum Technology, through the National Energy Technology Laboratory, under the U.S. Department of Energy, Contract No. DE-AC02-05CH11231. The authors are indebted to John Apps and Dan Hawkes for their careful review.

References

Anderson, B.J., Wilder, J.W., Kurihara, M., White, M.D., Moridis, G.J., Wilson, S.J., Pooladi-Darvish, M., Masuda, Y., Collett, T.S., Hunter, R.B., Narita, H., Rose, K. and Boswell, R., 2008. Analysis of Modular Dynamic Formation Test Results From the Mount Elbert-01 Stratigraphic Test Well, Milne Point Unit, North Slope, Alaska**,** paper presented at the 6th International Conference on Gas Hydrates, Vancouver, British Columbia, Canada, July 6-10, 2008.

Anderson, B., Hancock, S., Collett, T., Wilson, S., Boswell, R., Hunter, R., and Batzle, M., (this volume), MDT Operational summary, history matching, and interpretation.

Boswell, R., Hunter, R., Collett, T.S., Digert, S., Hancock, S., Weeks, M., and Mount Elbert Science Team, 2008, Investigation of gas hydrate bearing sandstone reservoirs at the Mount Elbert stratigraphic test well, Milne Point, Alaska: *Proceedings of the 6th International Conference on Gas Hydrates*, July 6-10, 2008, Vancouver, British Columbia, Canada.

Bird, K.J., and Magoon, L.B., 1987, Petroleum geology of the northern part of the Arctic National Wildlife Refuge, Northeastern Alaska: *U.S. Geological Survey Bulletin* **1778**, 324.

Clarke, M.A., and Bishnoi, P.R., 2000. Determination of the Intrinsic Rate of Methane Gas Hydrate Decomposition", *Chem. Eng. Sci.*, **55**, 4869.

Collett, T.S., Bird, K.J., Kvenvolden, K.A., and Magoon, L.B., 1988, Geologic interrelations relative to gas hydrates within the North Slope of Alaska: U.S. *Geological Survey Open-File Report 88-389*, 150.

Collett, T., 1993, Natural gas hydrates of the Prudhoe Bay and Kuparuk River area, North Slope, Alaska: *American Association of Petroleum Geologists Bulletin*, **77** (5), 793-812.

Collett, T., 1995. *1995 National Assessment of U.S. Oil and Gas Resources* (on CD-ROM) (Gautier, D.L., Goldton, G.L. et al., eds.), USGS.

Collett, T., 2007. Arctic Gas Hydrate Energy Assessment Studies, The Arctic Energy Summit, Anchorage, Alaska, 15-18 October 2007.

Collett, T., Lewis, R., Rose, K., Hunter, R., Boswell, R., and Winters, W., (this volume), Well logging operations and core/log data integration, BPXA-DOE-USGS Mount Elbert Gas Hydrate Stratigraphic Test Well.

Dallimore, S.R., Uchida, T., and Collett, T.S., 1999, Scientific results from JAPEX/JNOC/GSC Mallik 2L-38 gas hydrate research well, Mackenzie Delta, Northwest Territories, Canada, *Geological Survey of Canada Bulletin* **544**, 403.

Dallimore, S.R., and Collett, T.S., Eds., 2005. Scientific Results from the Mallik 2002 Gas Hydrate Production Research Well Program, Mackenzie Delta, Northwest Territories, Canada, *Geological Survey of Canada Bulletin* **585**.

Kim, H.C., Bishnoi, P.R., Heidemann, R.A., and Rizvi, S.S.H., 1987. Kinetics of Methane Hydrate Decomposition, *Chem. Eng. Sci*., **42**(7), 1645.

Klauda, J.B., and Sandler, S.I., 2005. Global distribution of methane hydrate in ocean sediment, *Energy & Fuels* **19**, 469.

Kowalsky, M. B., and Moridis, G.J., 2007, Comparison of kinetic and equilibrium reactions in simulating the behavior of gas hydrates, *Energy Conversion and Management*, **48**, 1850, doi:10.1016/j.enconman.2007.01.017 (LBNL-63357).

Kurihara, M., Funatsu, K., Ouchi, H., Masuda Y. and Narita, H., 2005b. Investigation On Applicability Of Methane Hydrate Production Methods To Reservoirs With Diverse Characteristics, Paper 3003 presented at the 5th International Conference on Gas Hydrates, Trondheim, Norway, 13–16 June, Proceedings, Vol. 3, 714-725.

Kurihara, M., Sato, A., Ouchi, H., Narita, H., Masuda, Y., Saeki, T., and Fujii, T. 2009. Prediction of Gas Productivity from Eastern Nankai Trough Methane-Hydrate Reservoirs. *SPE Res Eval & Eng* **12** (3): 477-499. SPE-125481-PA. doi: 10.2118/125481-PA.

Milkov, A. V., 2004. Global estimates of hydrate-bound gas in marine sediments: How much is really out there? *Earth Science Reviews* **66** (3), 183.

Makogon, Y.F., 1987. Gas hydrates: frozen energy, *Recherche* **18** (192), 1192.

Makogon, Y.F., 1997. *Hydrates of Hydrocarbons*. Penn Well Publishing Co. Tulsa, OK.

Moridis, G.J., 2003. Numerical Studies of Gas Production From Methane Hydrates, *SPE Journal*, **32**(8), 359.

Moridis, G.J., and Sloan, E.D., 2007. Gas Production Potential of Disperse Low-Saturation Hydrate Accumulations in Oceanic Sediments, *J. Energy Conversion and Management*, **48** (6), 1834-1849.

Moridis, G.J., Collett, T., Dallimore, S., Satoh, T., Hancock, S., and Weatherhill, B., 2004. Numerical Studies Of Gas Production From Several Methane Hydrate Zones At The Mallik Site, Mackenzie Delta, Canada, *JPSE* **43**, 219.

Moridis, G.J., and Reagan, M.T., 2007a. Strategies for Gas Production From Oceanic Class 3 Hydrate Accumulations, *OTC-18865*, 2007 Offshore Technology Conference, Houston, Texas, 30 April – 3 May 2007.

Moridis, G.J., and Reagan, M.T., 2007b. Gas Production From Oceanic Class 2 Hydrate Accumulations, *OTC 18866*, 2007 Offshore Technology Conference, Houston, Texas, U.S.A., 30 April–3 May 2007.

Moridis, G.J., and Reagan, M.T., 2007c. Gas Production From Class 2 Hydrate Accumulations in the Permafrost, *SPE 110858*, 2007 SPE Annual Technical Conference and Exhibition, Anaheim, California, U.S.A., 11–14 November 2007.

Moridis, G.J., Collett, T.S., Boswell, R., Kurihara, M., Reagan, M.T., Koh, C., Sloan, E.D., 2008a. Toward Production from Gas Hydrates: Status, Technology, and Potential, SPE 114163, SPE Unconventional Reservoirs Conference, Keystone, Colorado, U.S.A., 10–12 February 2008.

Moridis, G.J., Kowalsky, M., and Pruess, K., 2008b. Depressurization-Induced Gas Production From Class 1 Hydrate Deposits, *SPE Reservoir Evaluation and Engineering*, **10** (5), 458-488.

Moridis, G.J., Kowalsky, M.B., and Pruess, K., 2008c. TOUGH+HYDRATE v1.0 User's Manual: A Code for the Simulation of System Behavior in Hydrate-Bearing Geologic Media, Report LBNL-00149E, Lawrence Berkeley National Laboratory, Berkeley, CA.

Reagan, M.T., Moridis, G.J., and Zhang, K., 2008. Sensitivity Analysis of Gas Production from Class 2 and Class 3 Hydrate Deposits, OTC 19554, 2008 Offshore Technology Conference, Houston, Texas, USA, 5-8 May 2008.

Sloan, E.D., and Koh, C., 2008. *Clathrate Hydrates of Nautral Gases.* 3rd Edition, Taylor and Francis, Inc., Boca Raton, FL.

Sun, X., and Mohanty, K.K., 2005. Simulation of Methane Hydrate Reservoirs, SPE 93015, 2005 SPE Reservoir Simulation Symposium, Houston, TX U.S.A., 31 January - 2 February 2005.

van Genuchten, M.Th., 1980. A Closed-Form Equation for Predicting the Hydraulic Conductivity of Unsaturated Soils", *Soil Sci. Soc.*, **44**, 892.

White, M., 2008. Personal communication.

Wright, J.F., Dallimore, S.R., and Nixon, F.M., 1999. Influences of Grain Size and Salinity on Pressure-Temperature Thresholds for Methane Hydrate Stability in JAPEX/JNOC/GSC Mallik 2L-38 Gas Hydrate Research-Well Sediments, in Scientific Results from JAPEX/JNOC/GSC Mallik 2L-38 Gas Hydrate Research-Well, Mackenzie Delta, Northwest Territories, Canada. Dallimore, S.R., Uchida, T., and Collett, T.S., Eds., *Geological Survey of Canada Bulletin* **544**, 229.

Zhang, K., and Moridis, G.J., 2008. A Domain Decomposition Approach for Large-Scale Simulations of Coupled Processes in Hydrate-Bearing Geologic Media**,** paper presented at the 6th International Conference on Gas Hydrates, Vancouver, British Columbia, Canada, July 6-10, 2008.

Table 1 – Hydrate Deposit Properties in unit D, Mount Elbert Site

Parameter	Value
Hydrate zone thickness	11.3 m
Initial pressure at top of HBL (P_T)	6.386 MPa
Initial temperature at top of HBL (T_T)	2.3 ^{o}C
Initial temperature at base of HBL (T_B)	2.6 ^{o}C
Gas composition	100% CH_4
Initial saturations in the HBL	S_H = 0.65, S_A = 0.35
Intrinsic permeability of HBL $k_r = k_x = k_z$	10^{-12} m^2 (= 1 D)
Porosity of HBL ϕ	0.4
Compressibility of HBL	5x10^{-9} Pa^{-1}
Intrinsic permeability $k_r = k_x = k_z$ (overburden & underburden)	0 m^2 (= 0 D)
Porosity of overburden & underburden	0.005
Grain density ρ_R (all formations)	2750 kg/m^3
Constant bottomhole pressure (P_w)	3 MPa
Dry thermal conductivity ($k_{\Theta RD}$) (all formations)	0.5 W/m/K
Wet thermal conductivity ($k_{\Theta RW}$) (all formations)	3.1 W/m/K
Composite thermal conductivity model (Moridis et al., 2008c)	$k_{\Theta C} = k_{\Theta RD} + (S_A^{1/2} + S_H^{1/2})\,(k_{\Theta RW} - k_{\Theta RD}) + \phi\, S_I\, k_{\Theta I}$
Capillary pressure model (vanGenuchten, 1980)	$P_{cap} = -P_0 \left[\left(S^* \right)^{-1/\lambda} - 1 \right]^{\lambda}$ $S^* = \frac{(S_A - S_{irA})}{(S_{mxA} - S_{irA})}$
S_{irA}	1
λ (White, 2008)	0.77437
P_0 (White, 2008)	5x10^3 Pa
Relative permeability model (Moridis et al., 2008c)	$k_{rA} = (S_A^*)^n$ $k_{rG} = (S_G^*)^m$ $S_A^* = (S_A - S_{irA})/(1 - S_{irA})$ $S_G^* = (S_G - S_{irG})/(1 - S_{irA})$ EPM model
n; m (from Anderson et al., 2008)	4.2; 2.5
S_{irG}	0.02
S_{irA}	0.20

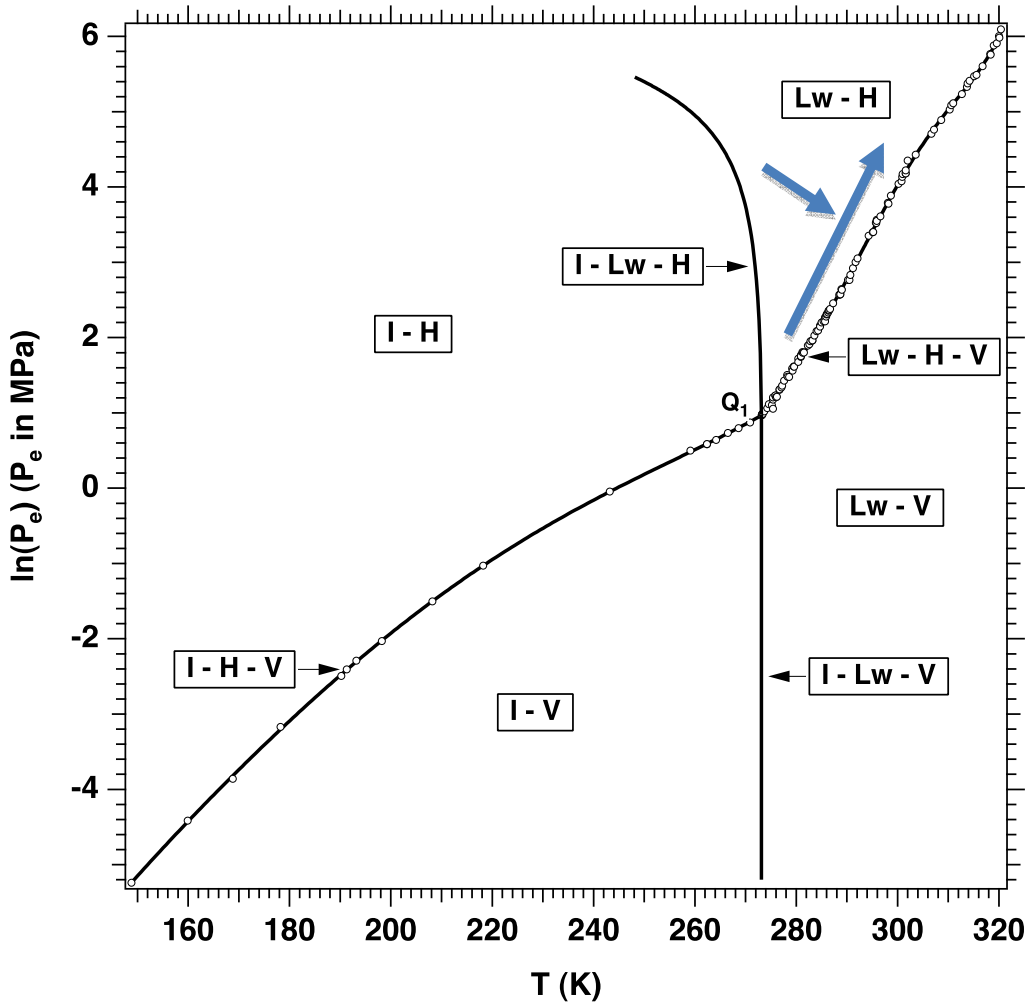

Figure 1.1. Pressure-temperature equilibrium relationship in the phase diagram of the water–CH_4–hydrate system (Moridis, 2003), Lw: Liquid water; H: Hydrate; V: Vapor (gas phase); I: Ice; Q_1: Quadruple point (= I + Lw + H + V). The two arrows show the direction of increasing thermodynamic desirability of a deposit as a production target.

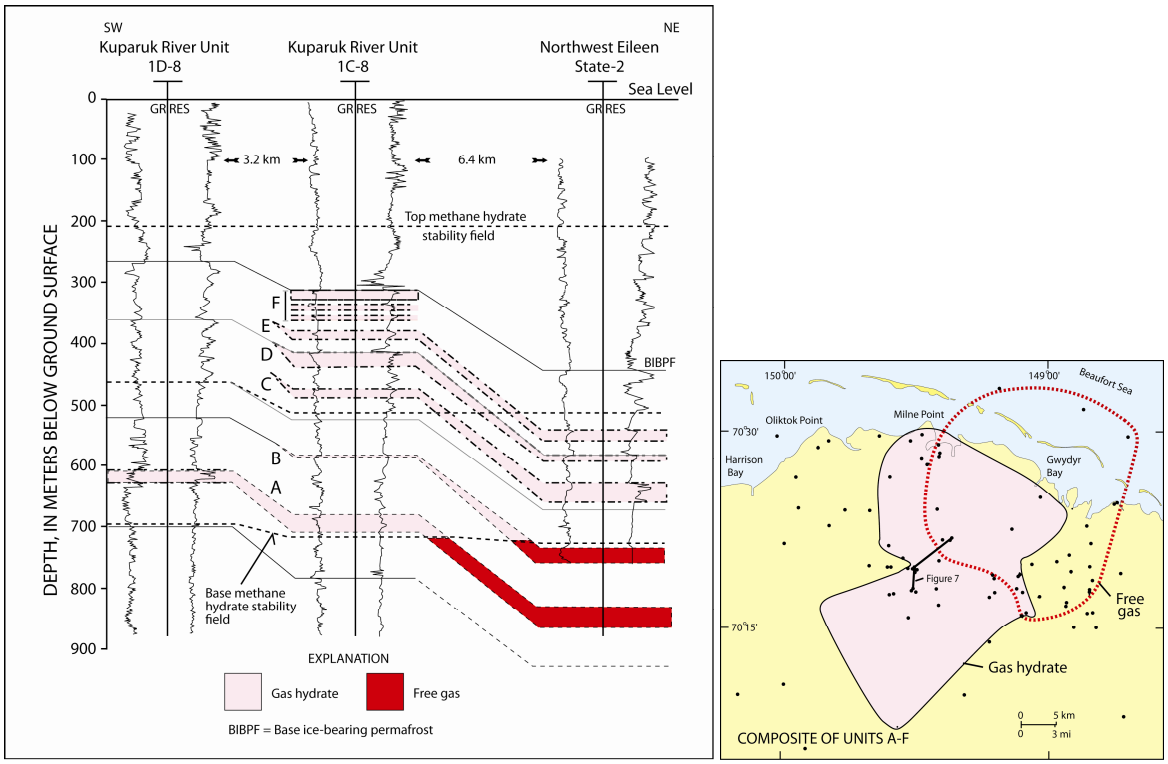

Figure 2.1. (a) Cross section showing the lateral and vertical extent of gas hydrates and underlying free-gas occurrences in the Prudhoe Bay-Kuparuk River area in northern Alaska. See Figure 2.1(b) for location of cross section. The gas-hydrate-bearing units are identified with the reference letters A through F (Collett, 1993), and their positions relative to the permafrost and to the base of the hydrate stability zone are shown; (b) Composite map of all six gas-hydrate/free-gas units (units A-F) from the Prudhoe Bay-Kuparuk River area in northern Alaska (Collett, 1993).

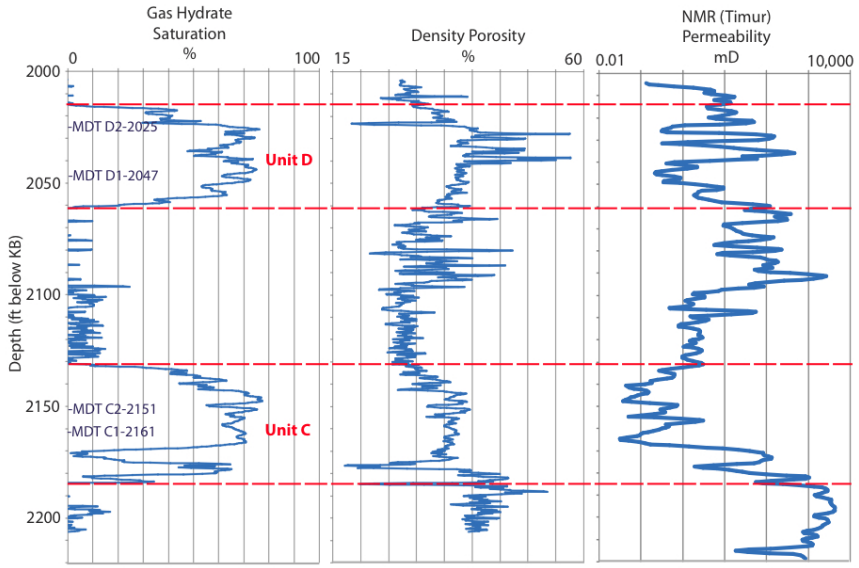

Figure 2.2. Relation of the C and D units at the Mount Elbert-01 well. The locations of the MDT tests in the two units are also shown.

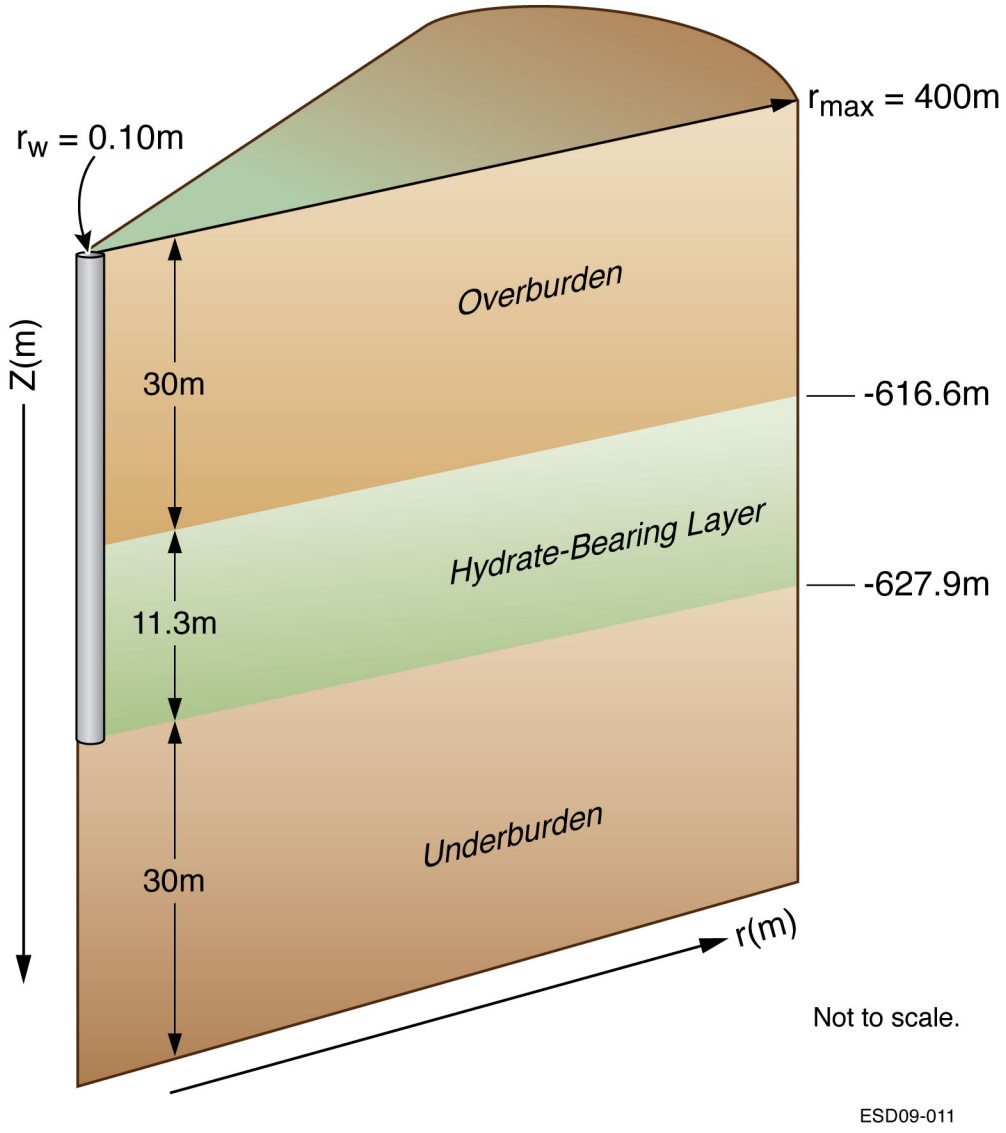

Figure 3.1. System geometry and configuration of the single vertical well producing from a cylindrical section of the Unit D Class 3 hydrate deposit at the Mount Elbert site.

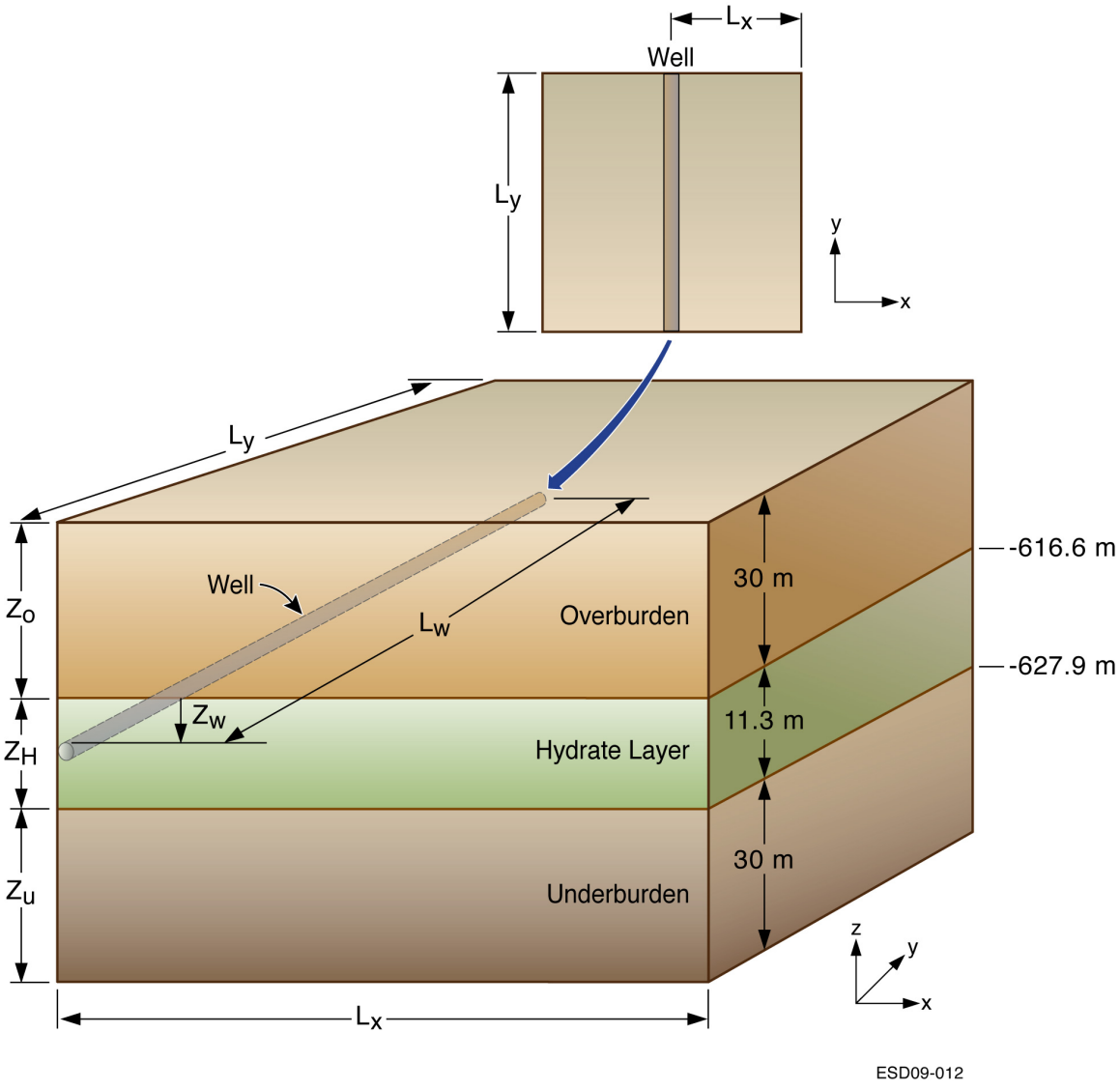

Figure 3.2. System geometry and configuration of the horizontal well producing from a rectangular section of the Unit D hydrate deposit that has the same area and hydrate volume as the cylindrical section of Figure 3.1 Note that $L_w = L_y$ = 709 m, $L_x = L_y/2$ = 354.5 m, Z_w = 0 m.

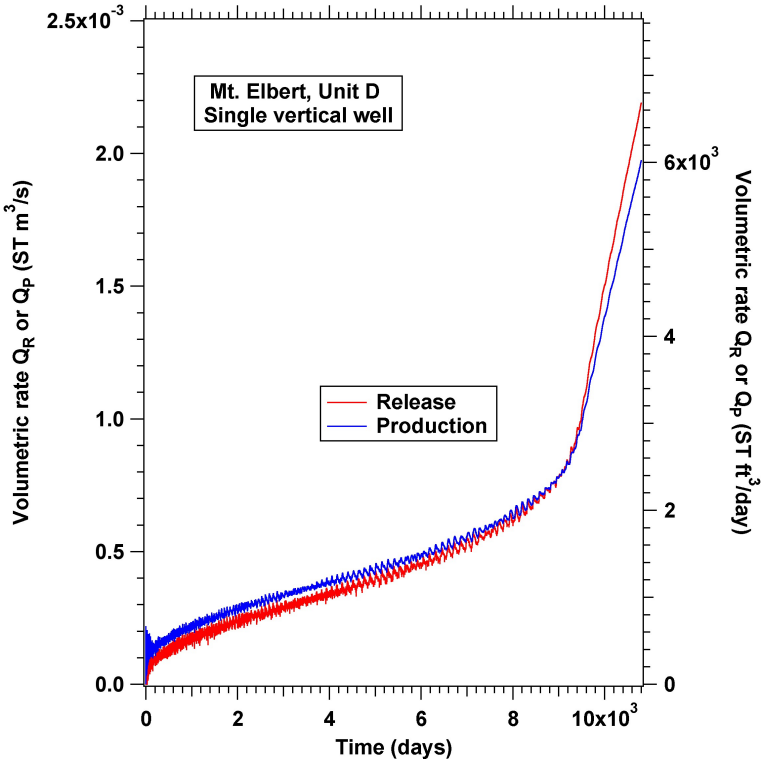

Figure 4.1. Evolution of Q_R and Q_P during production from Unit D using a vertical well.

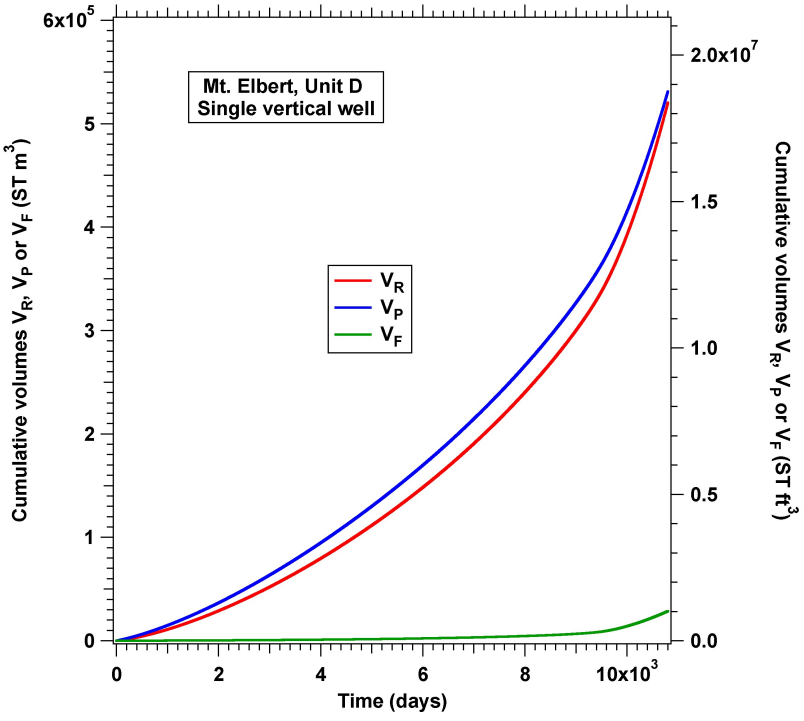

Figure 4.2. V_R, V_P and V_F during production from Unit D using a vertical well.

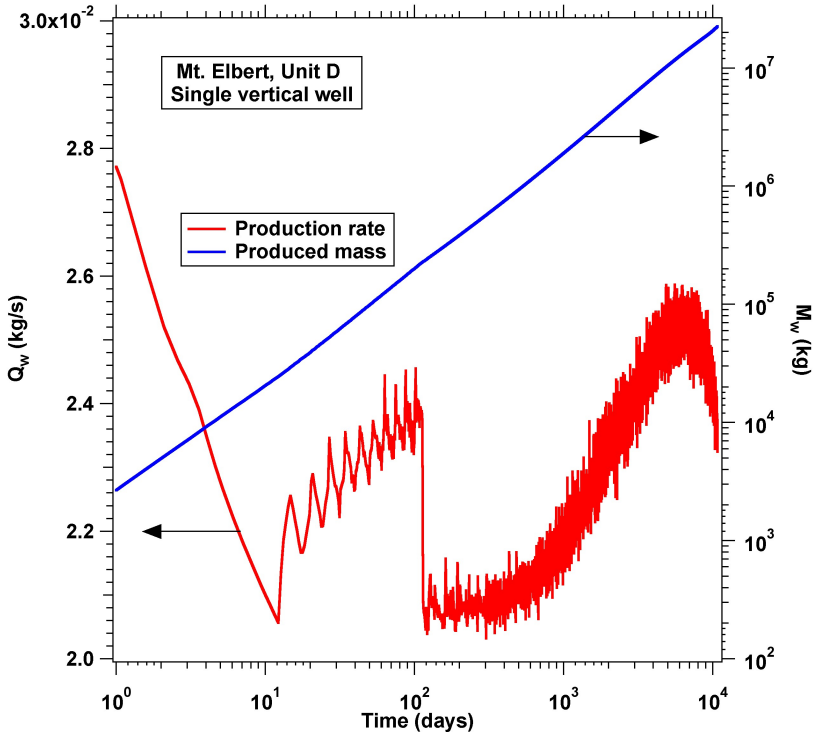

Figure 4.3. Evolution of Q_W and M_W during production from Unit D using a vertical well.

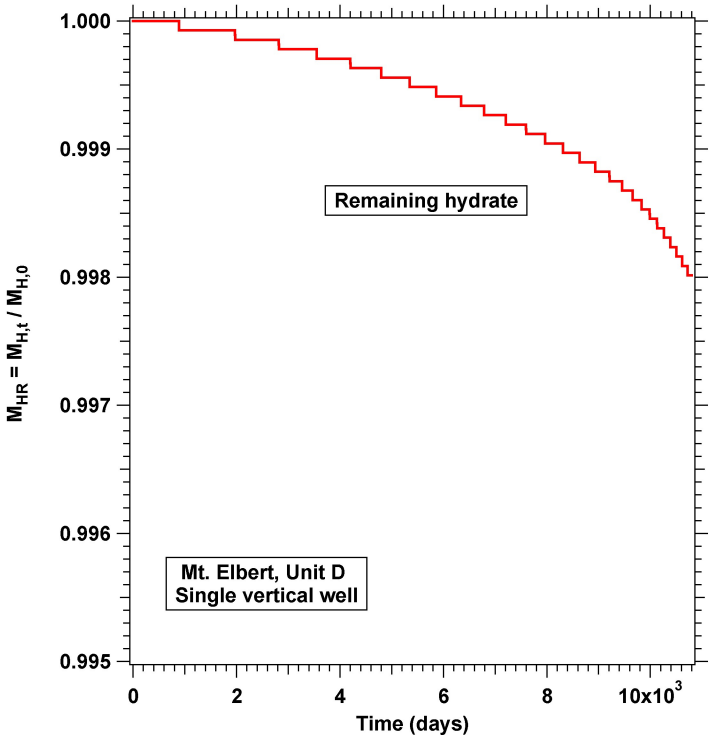

Figure 4.4. Fraction of remaining hydrate mass M_{HR} vs. time during production from Unit D using a vertical well. Note the negligible hydrate destruction after 30 years of continuous production.

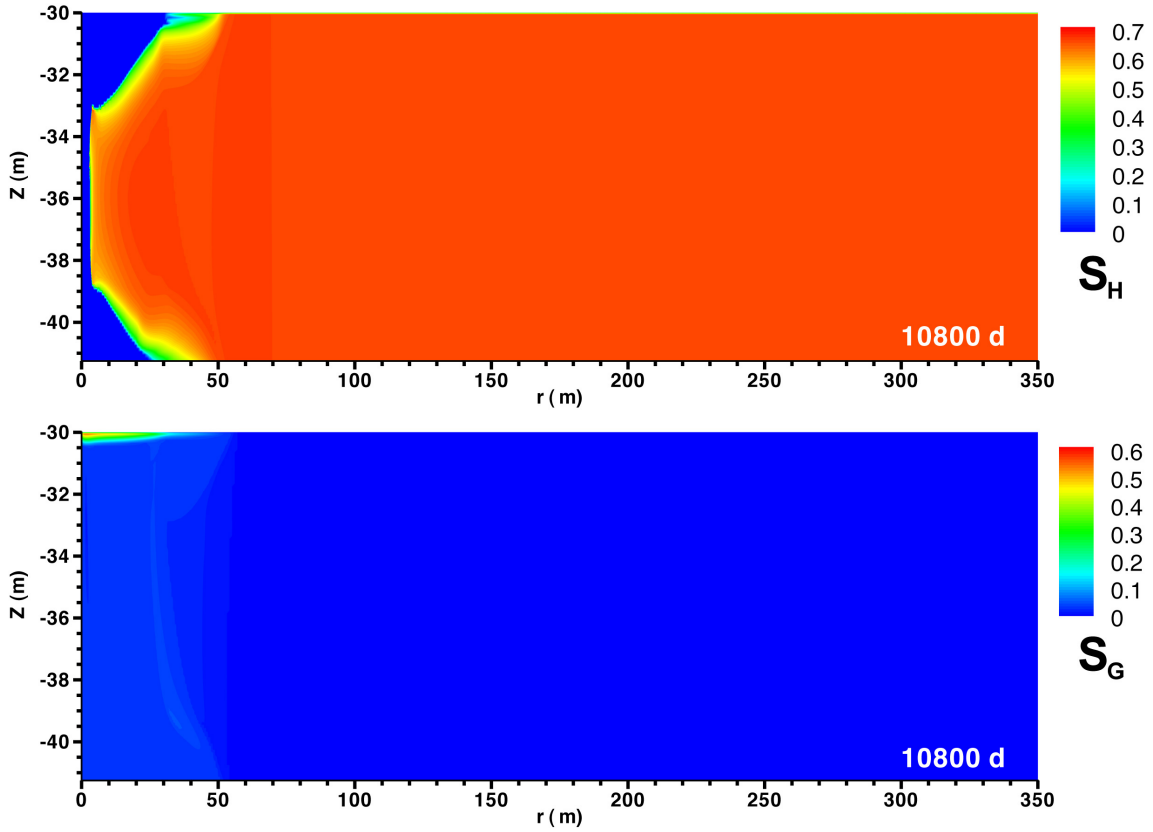

Figure 4.5. S_H and S_G profiles in Unit D after 30 years of continuous production using a vertical well.

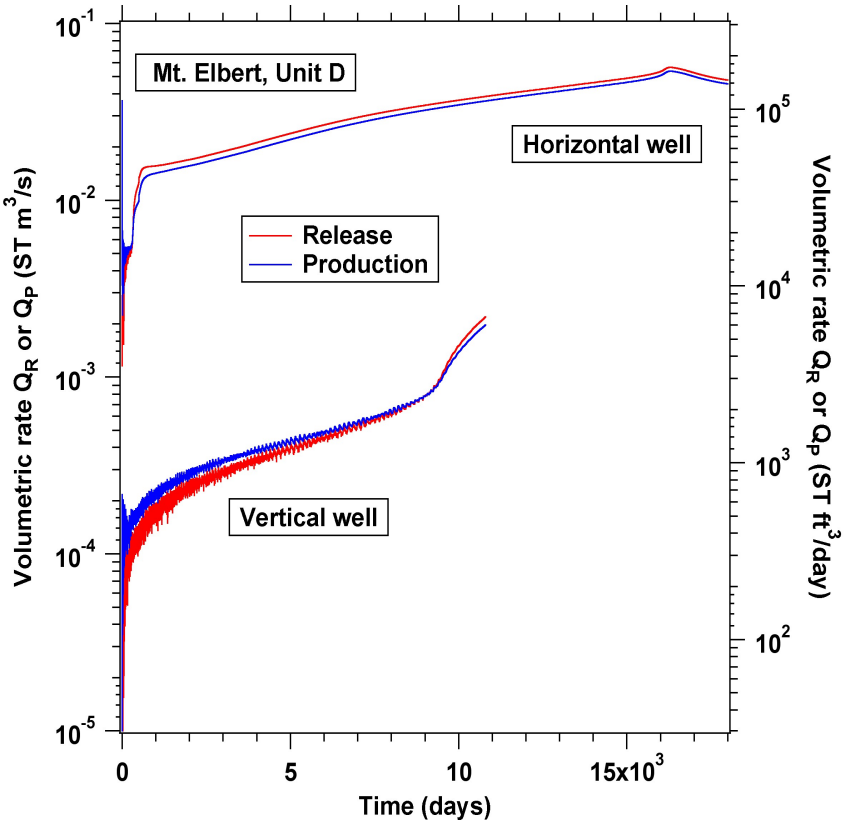

Figure 5.1. Comparison of Q_R and Q_P from a vertical and a horizontal well during production from Unit D.

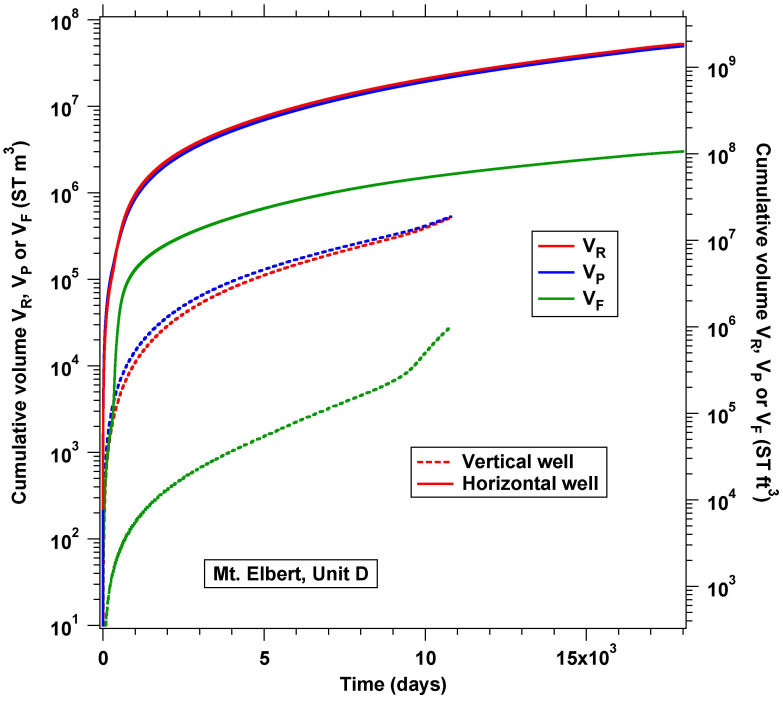

Figure 5.2. Comparison of V_R, V_P and V_F from a vertical and a horizontal well producing from Unit D.

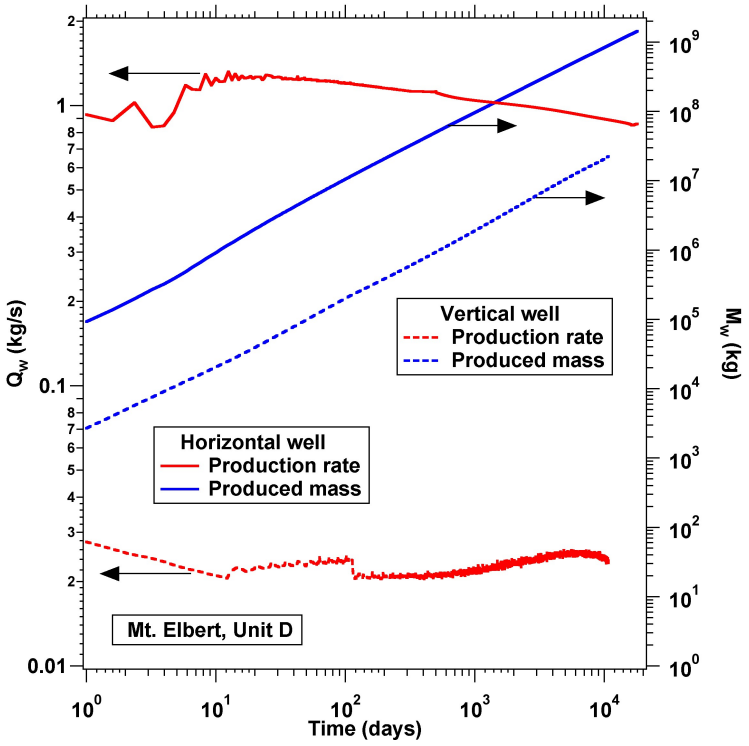

Figure 5.3. Comparison of Q_W and M_W from a vertical and a horizontal well during production from Unit D.

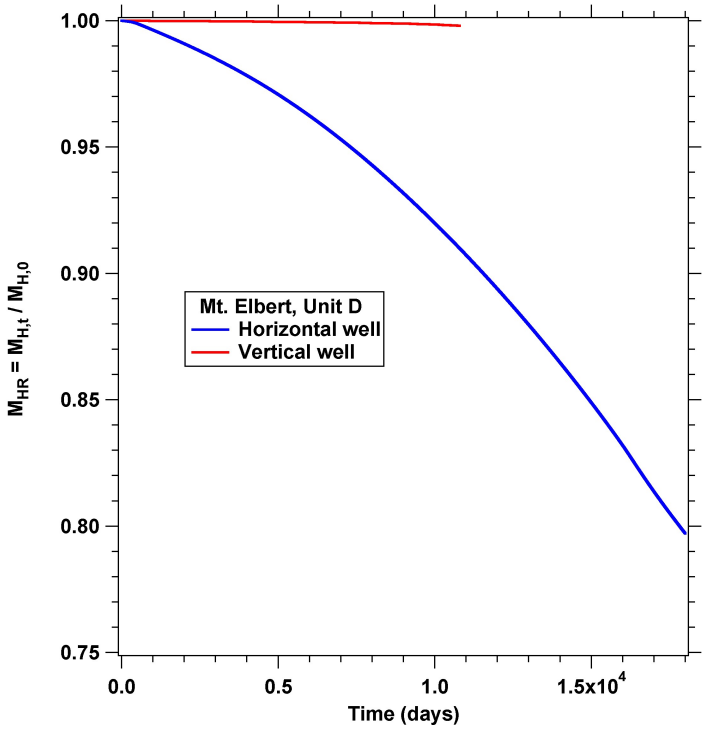

Figure 5.4. Comparison of evolution of M_{HR} from a vertical and a horizontal well during production from Unit D.

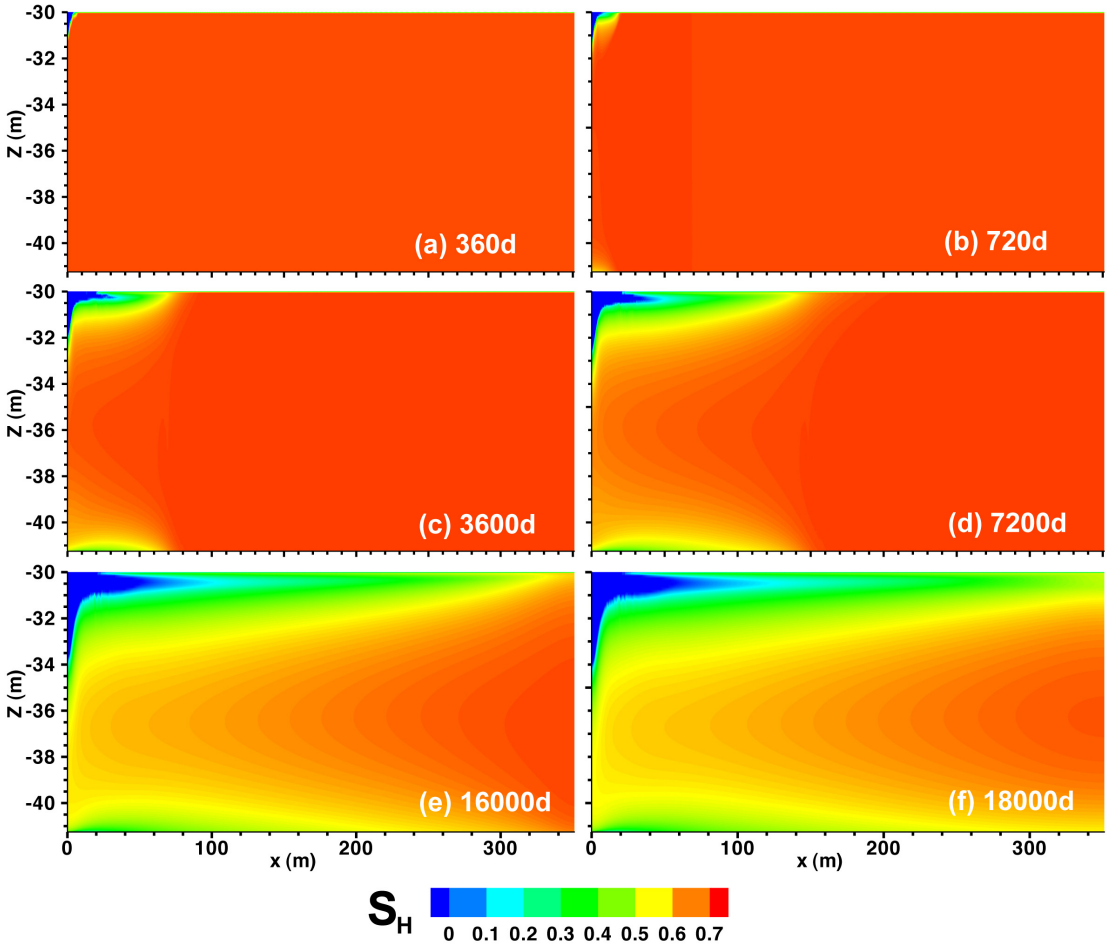

Figure 5.5. Evolution of the spatial distribution of S_H in Unit D during 50 years of continuous production using a horizontal well.

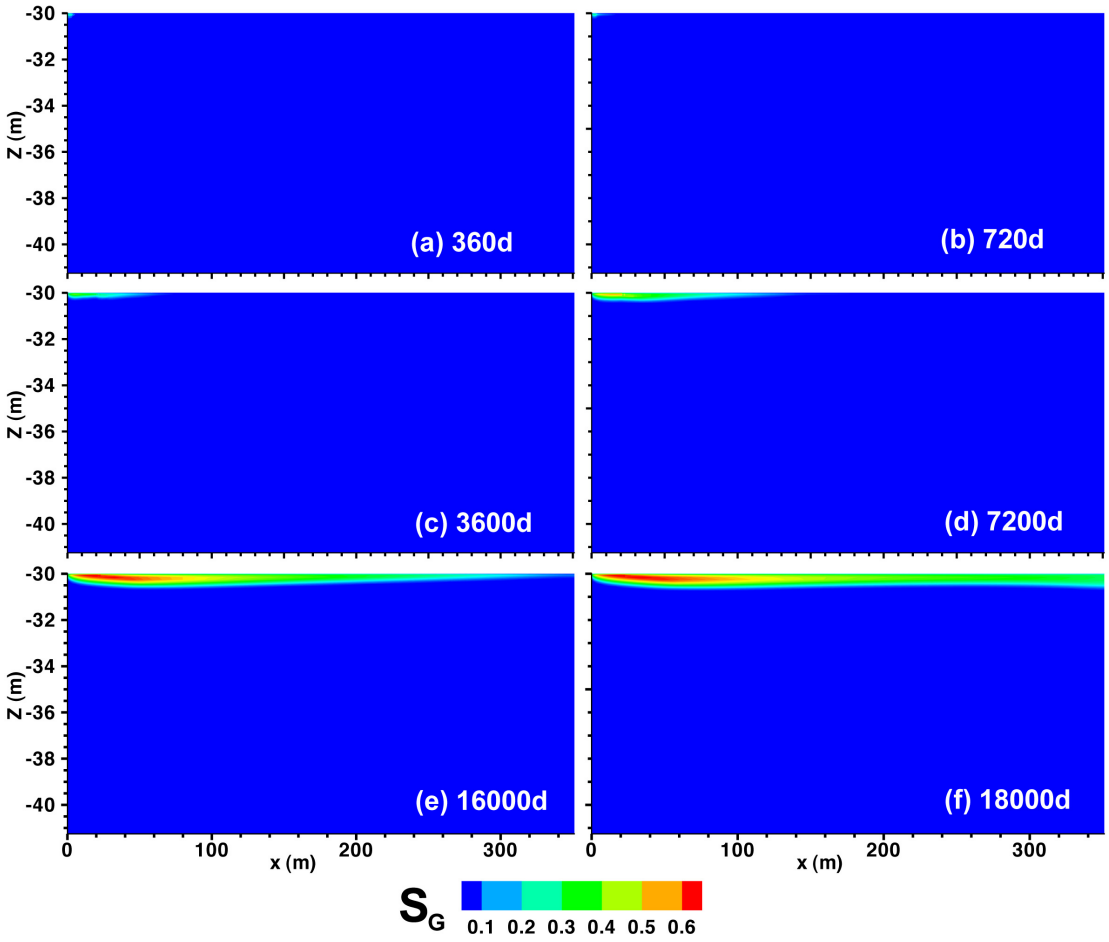

Figure 5.6. Evolution of the spatial distribution of S_G in Unit D during 50 years of continuous production using a horizontal well.

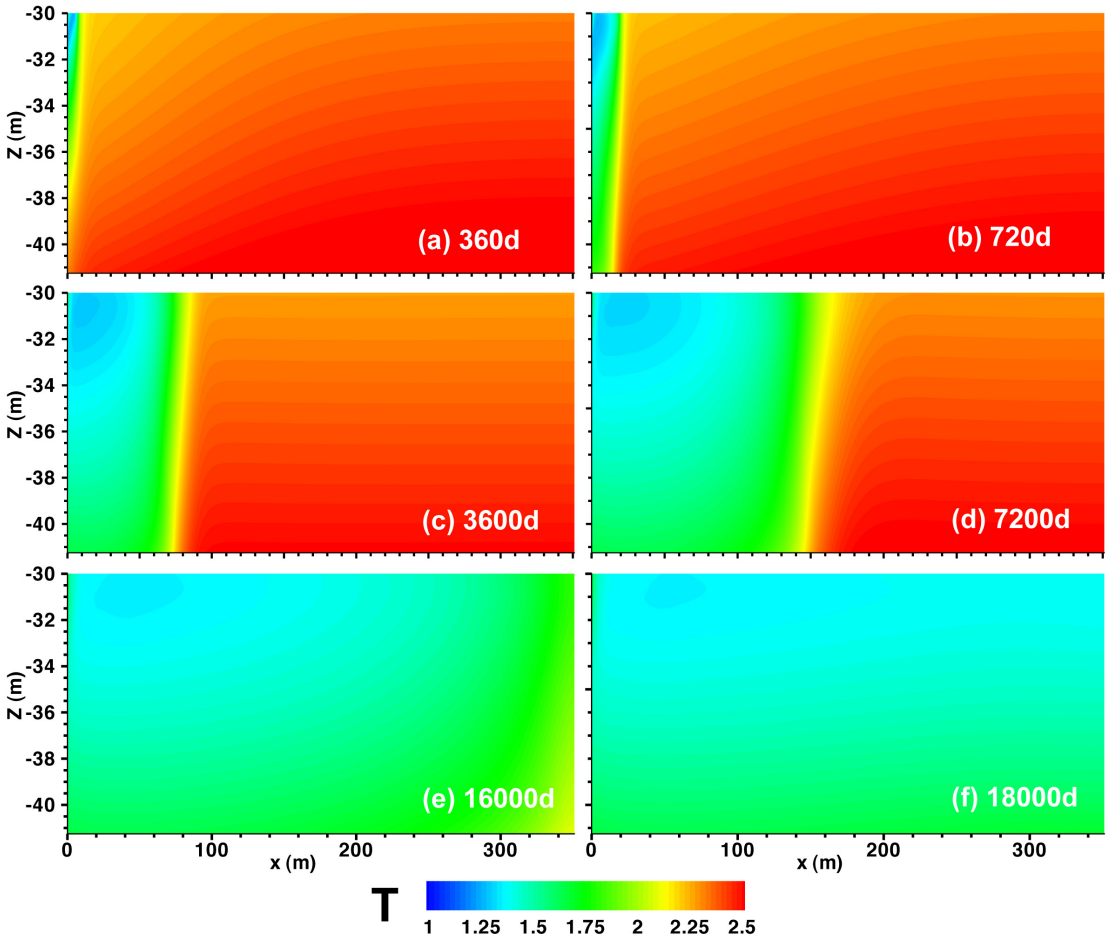

Figure 5.7. Evolution of the spatial distribution of T in Unit D during 50 years of continuous production using a horizontal well.

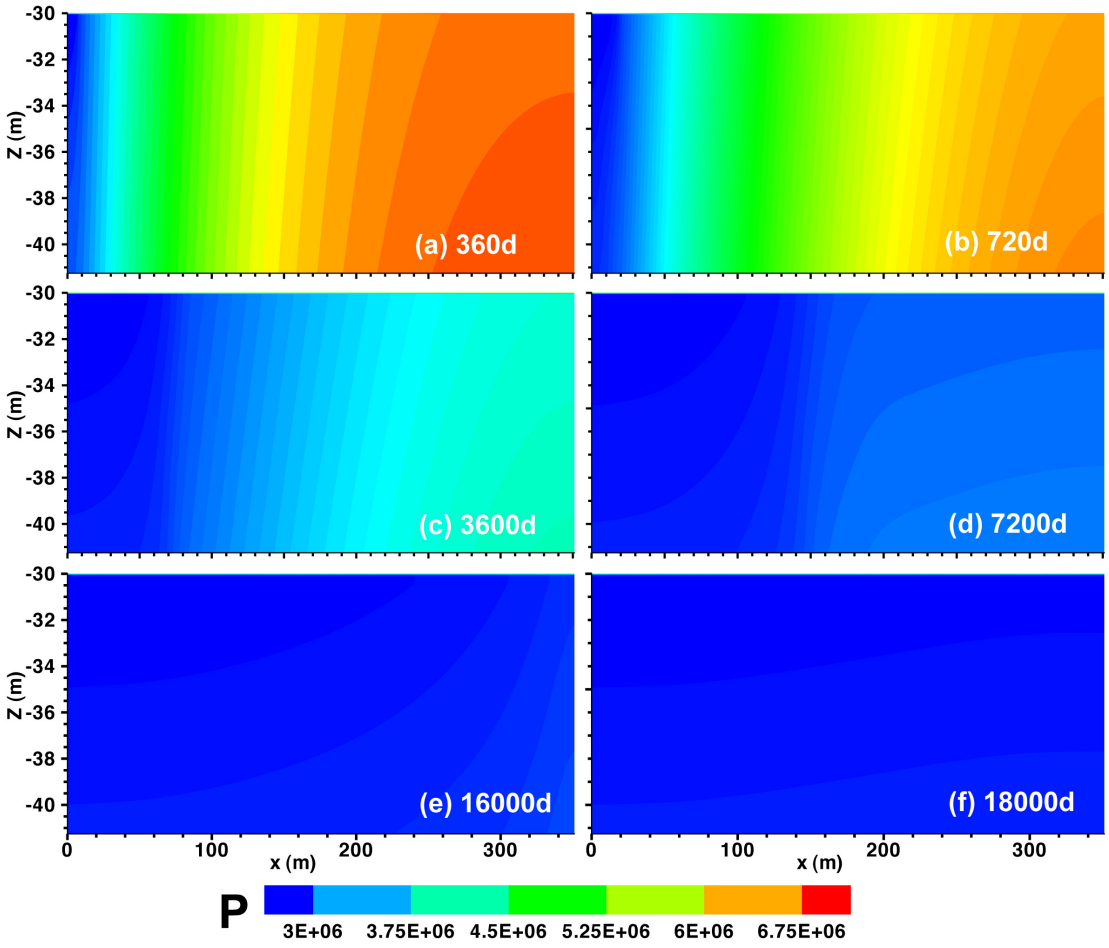

Figure 5.8. Evolution of the spatial distribution of P in Unit D during 50 years of continuous production using a horizontal well.

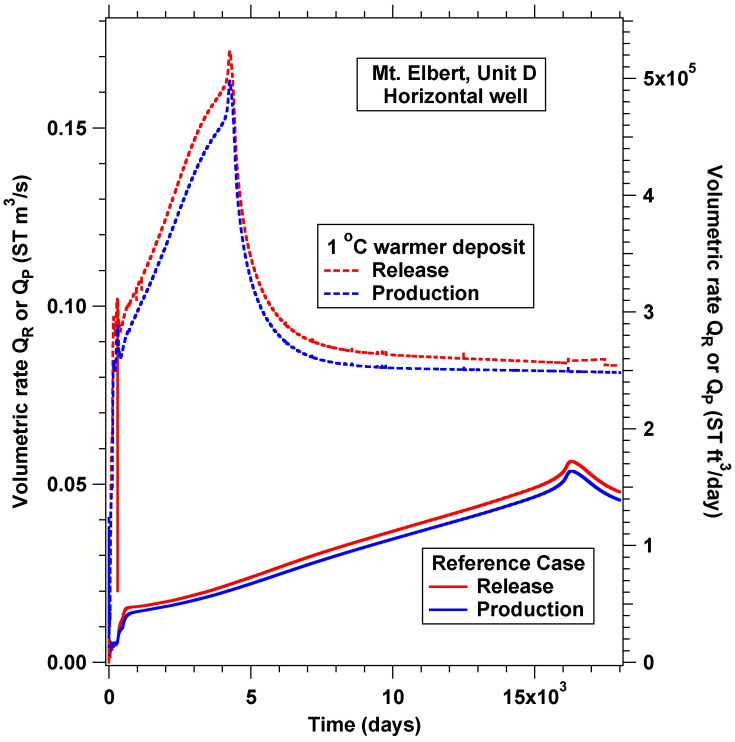

Figure 6.1. Sensitivity of Q_R and Q_P to the initial temperature of the deposit.

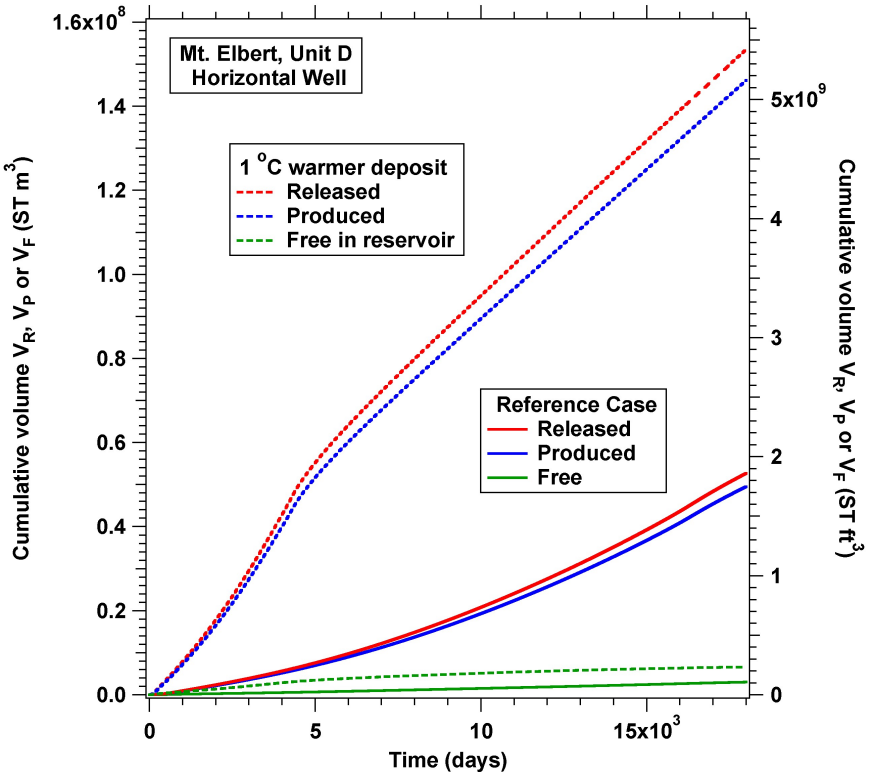

Figure 6.2. Sensitivity of Q_R, Q_P and Q_F to the initial temperature of the deposit.

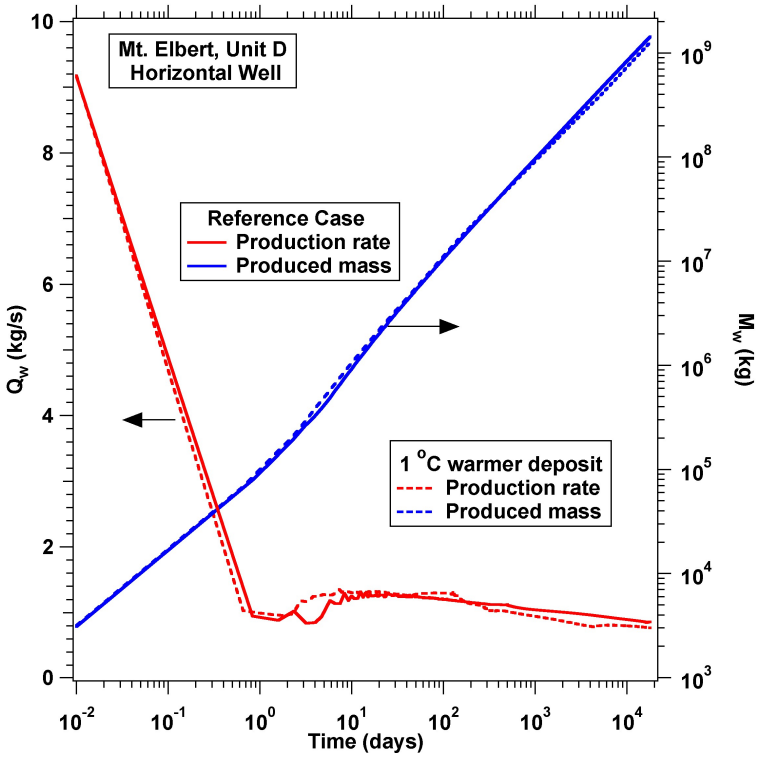

Figure 6.3. Sensitivity of Q_W and M_W to the initial temperature of the deposit.

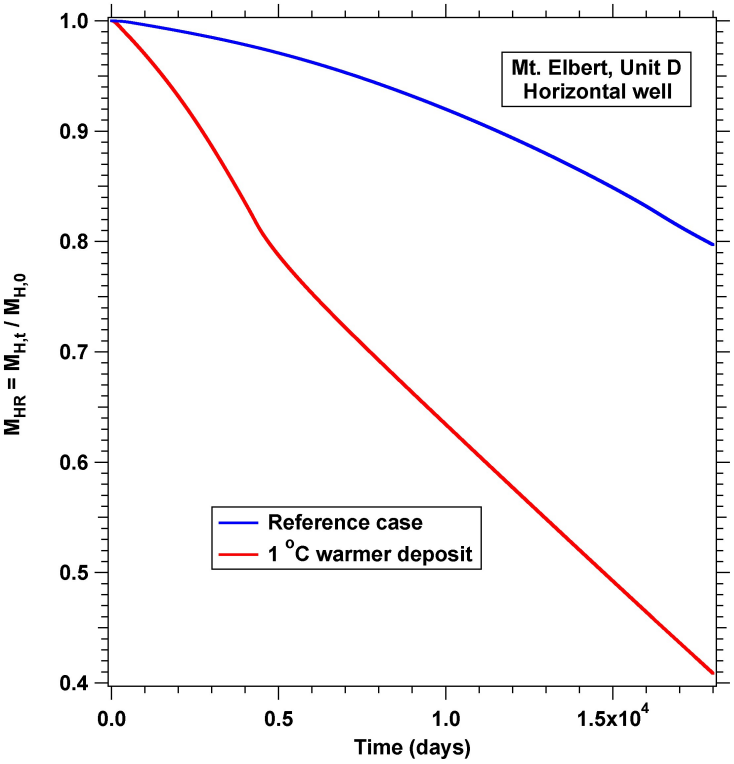

Figure 6.4. Sensitivity of M_{HR} to the initial temperature of the deposit.

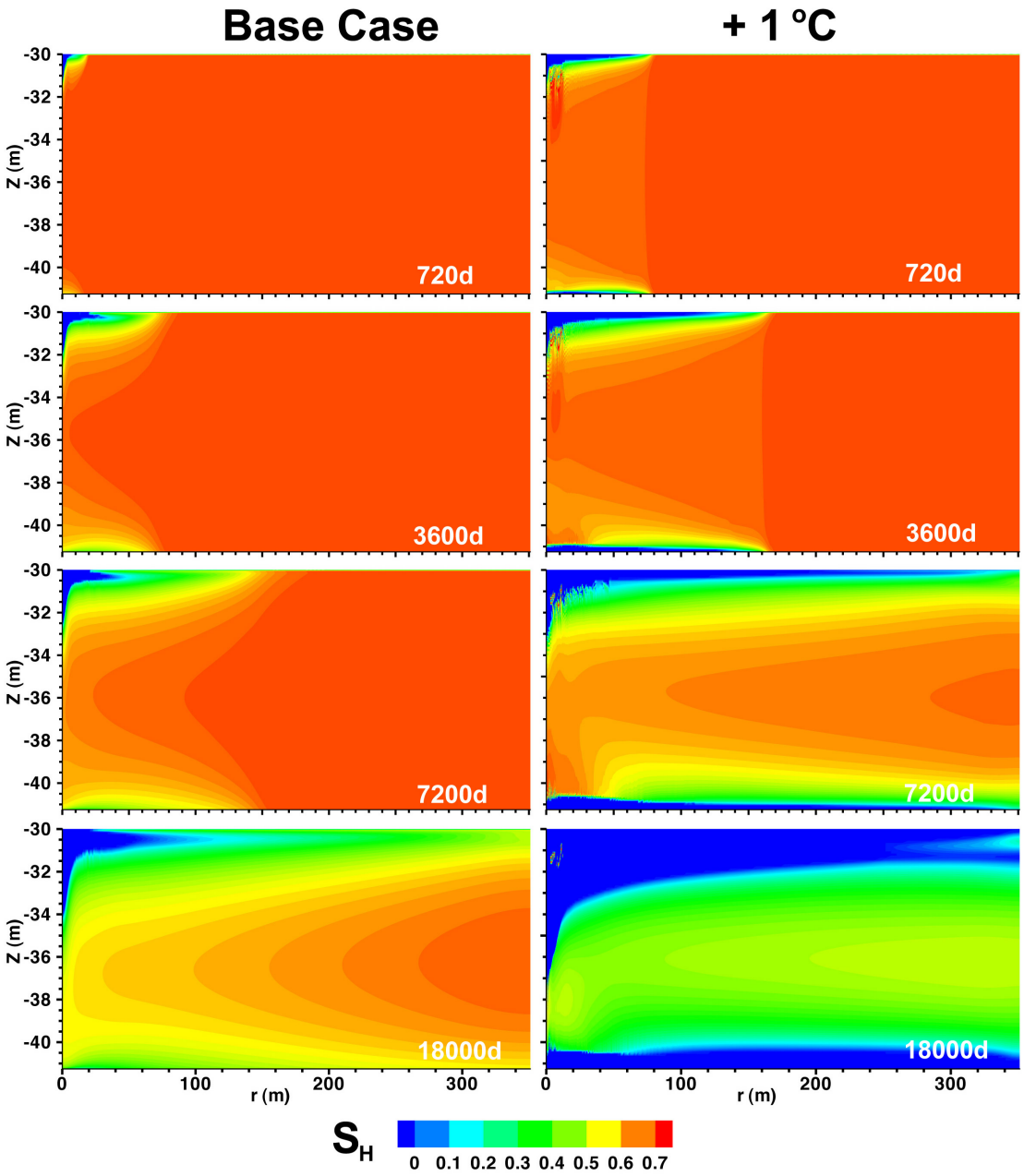

Figure 6.5. Effect of the initial temperature on the evolution of the spatial distribution of S_H in Unit D during 50 years of continuous production using a horizontal well.

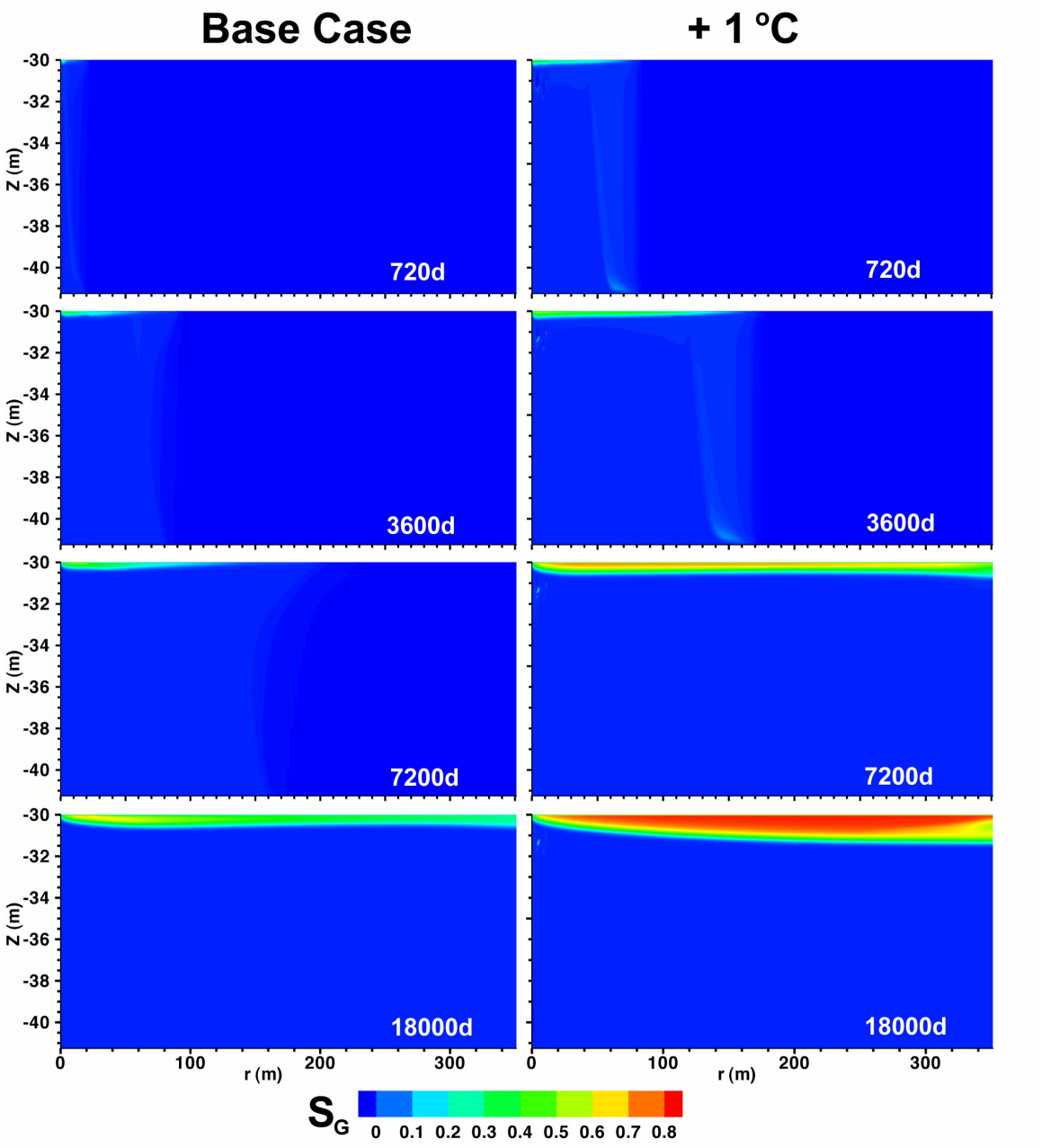

Figure 6.6. Effect of the initial temperature on the evolution of the spatial distribution of S_G in Unit D during 50 years of continuous production using a horizontal well.

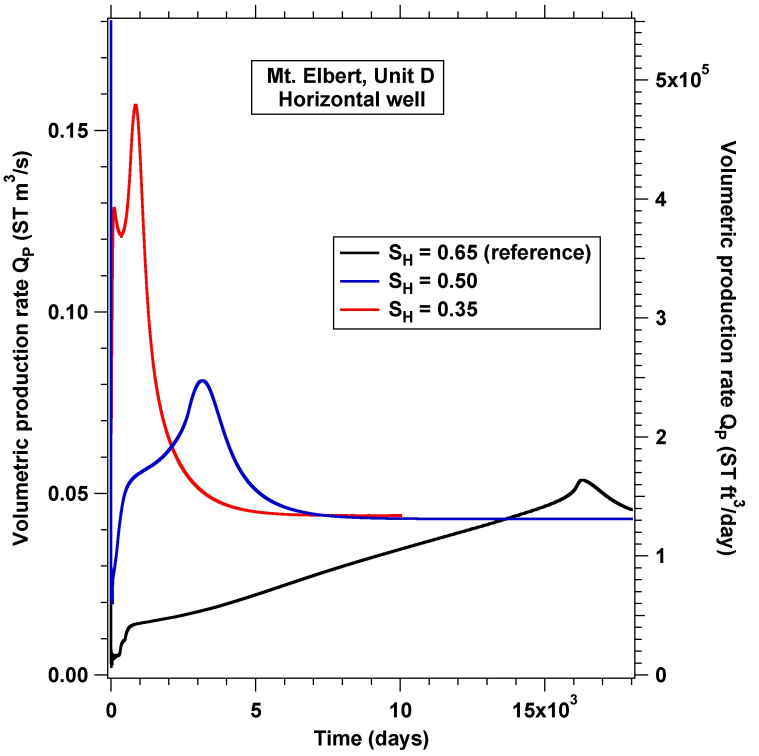

Figure 6.7. Sensitivity of Q_P to the initial S_H of the deposit.

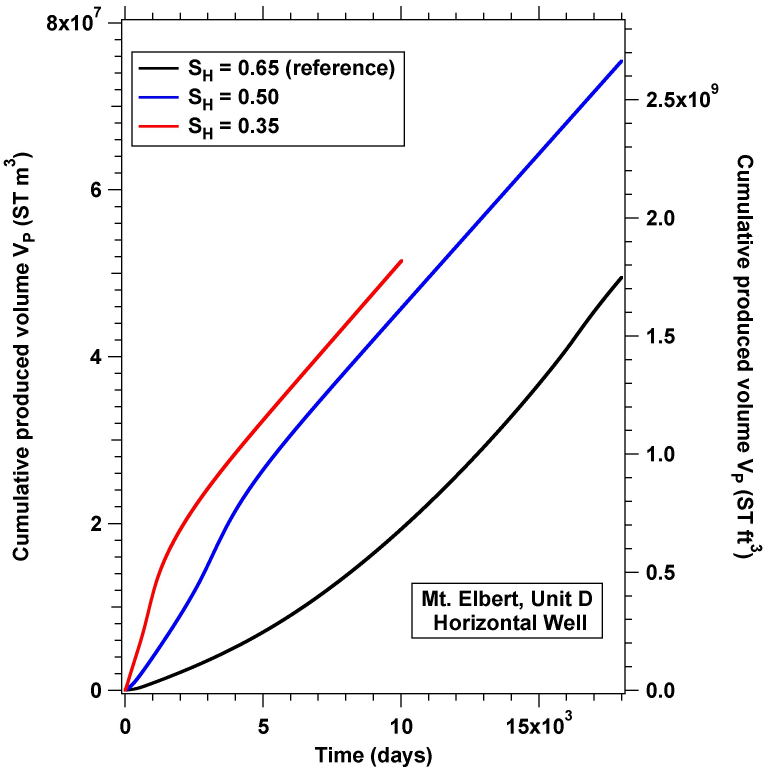

Figure 6.8. Sensitivity of V_P to the initial S_H of the deposit.

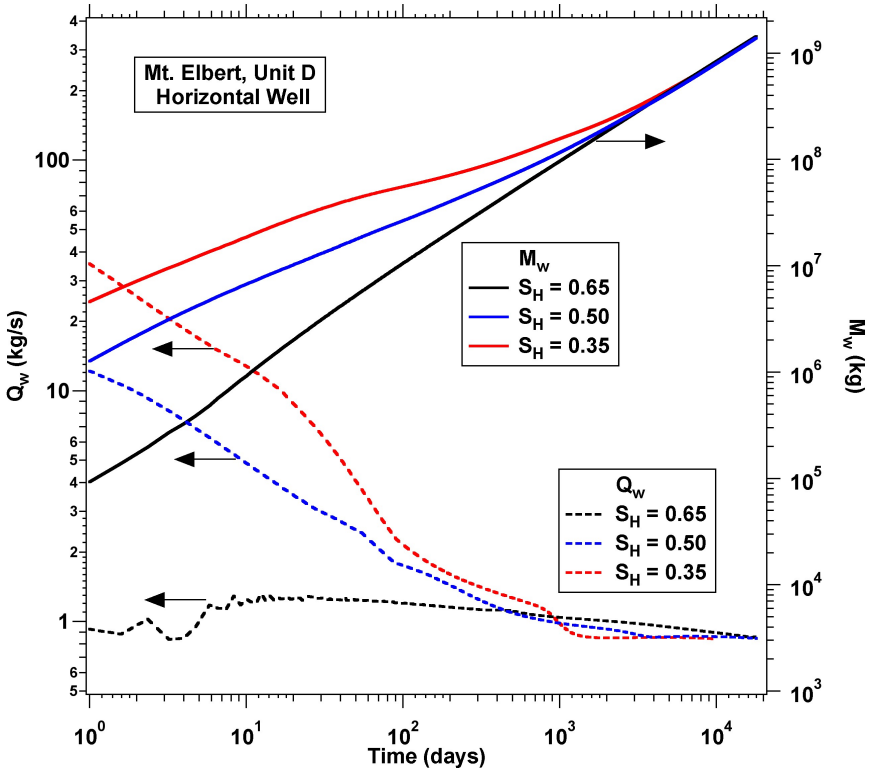

Figure 6.9. Sensitivity of Q_W and M_W to the initial S_H of the deposit.

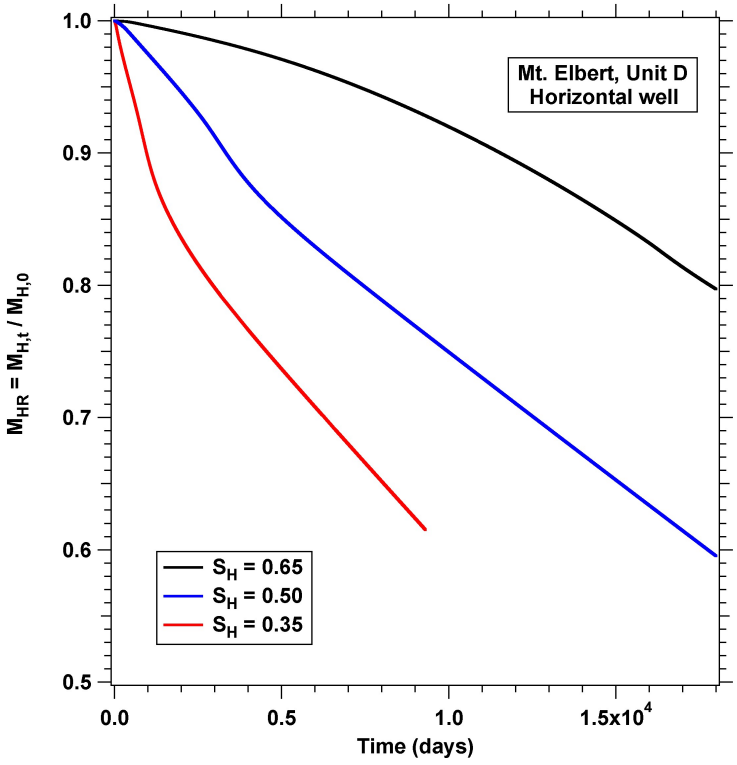

Figure 6.10. Sensitivity of M_{HR} to the initial S_H of the deposit.

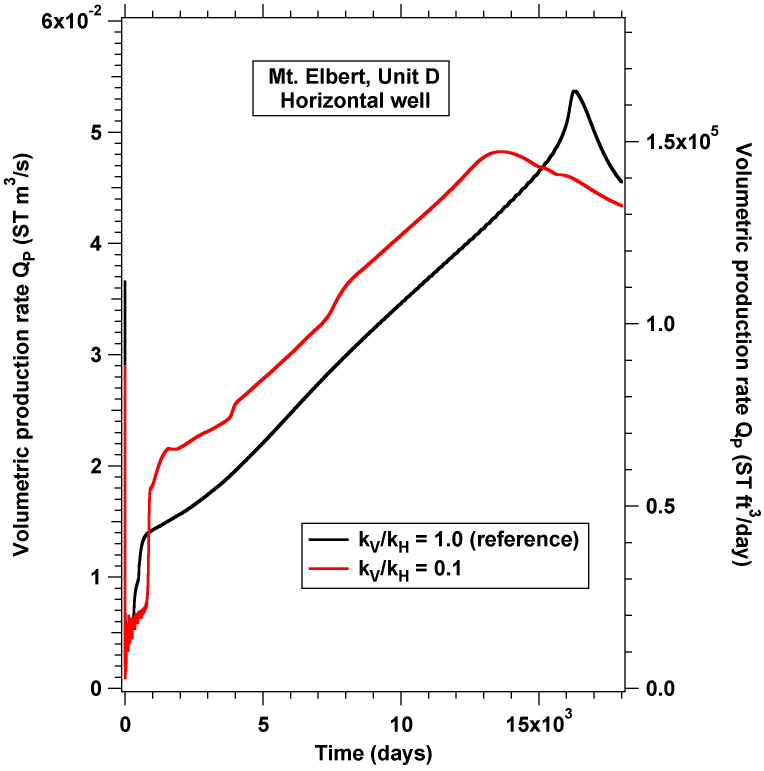

Figure 6.11. Sensitivity of Q_P to $k_R = k_V/k_H$.

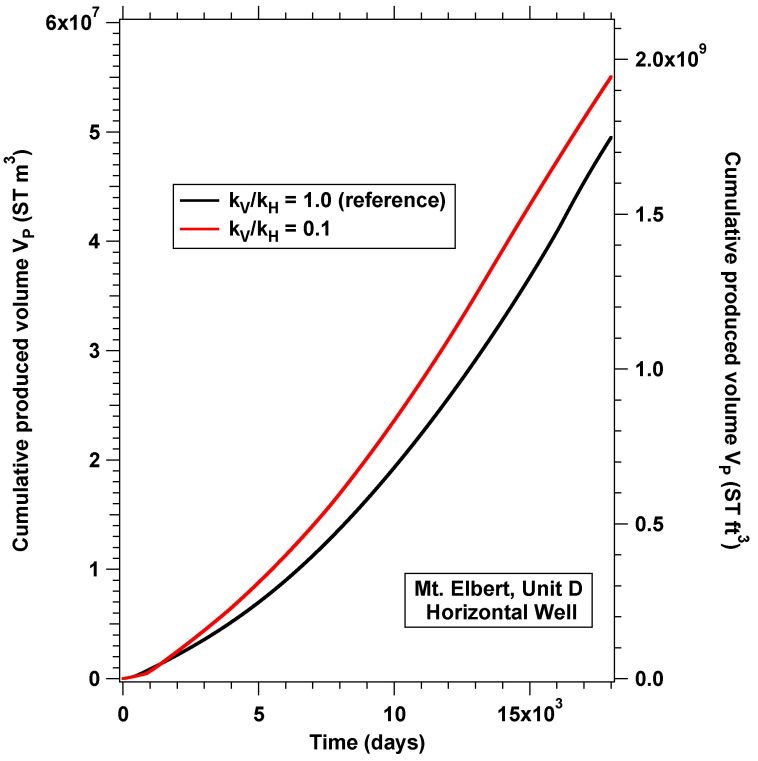

Figure 6.12. Sensitivity of V_P to $k_R = k_V/k_H$.

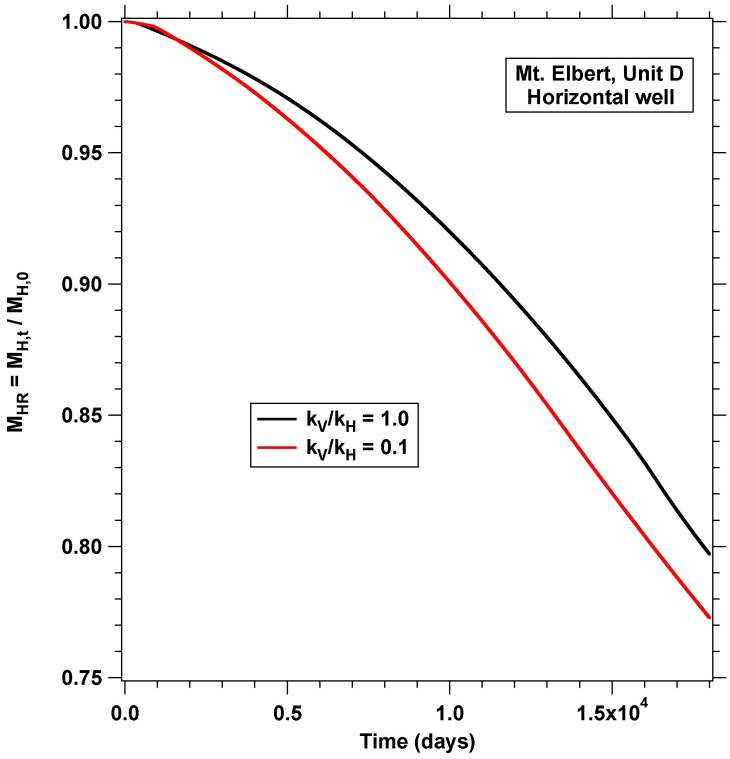

Figure 6.13. Sensitivity of M_{HR} to $k_R = k_V/k_H$.

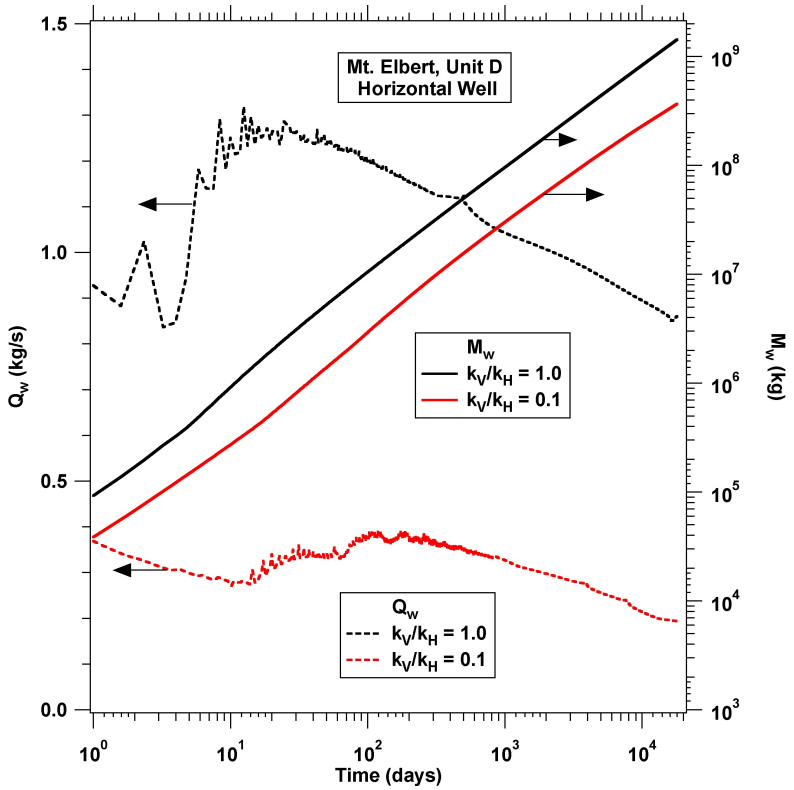

Figure 6.14. Sensitivity of Q_w and M_w to $k_R = k_V/k_H$.